

# Interferometry of black holes with Hawking radiation

Yasusada Nambu\*

*Department of Physics, Graduate School of Science,  
Nagoya University, Chikusa, Nagoya 464-8602, Japan*

Sousuke Noda†

*National Institute of Technology, Miyakonojo College, Miyakonojo 885-8567, Japan and*

*Center for Gravitation and Cosmology,  
College of Physical Science and Technology,  
Yangzhou University, Yangzhou 225009, China*

(Dated: September 14, 2021 ver 1.0)

## Abstract

We investigate wave optical imaging of black holes with Hawking radiation. The spatial correlation function of Hawking radiation is expressed in terms of transmission and reflection coefficients for scalar wave modes and evaluated by taking summation over angular quantum numbers numerically for the Unruh-Hawking state of the Kerr-de Sitter black hole. Then wave optical images of evaporating black hole are obtained by Fourier transformation of the spatial correlation function. For short wavelength, the image of the black hole with the outgoing mode of the Unruh-Hawking state looks like a star with its surface is given by the photon sphere. It is found that interference between incoming modes from the cosmological horizon and reflected modes due to scattering of the black hole can enhance brightness of images in the vicinity of the photon sphere. For long wavelength, whole field of view becomes bright and emission region of Hawking radiation cannot be identified.

Keywords: Hawking radiation; wave optics; van Citter-Zernike theorem; photon sphere; Kerr-de Sitter black hole

---

\*Electronic address: nambu@gravity.phys.nagoya-u.ac.jp

†Electronic address: snoda@cc.mykakojo-nct.ac.jp

## Contents

<b>I. Introduction</b>	2
<b>II. Van Citter-Zernike theorem and wave optical imaging</b>	4
A. Van Citter-Zernike theorem	4
B. Qubit detector and response functions	6
<b>III. Hawking radiation in Kerr-de Sitter spacetime</b>	7
A. Basic formulas	7
B. Correlation function	10
<b>IV. Evaluation of transmission and reflection coefficients</b>	13
<b>V. Imaging of black holes with Hawking radiation</b>	15
A. Detail of imaging method and an example with a simple model	15
B. Black hole images	18
1. Images for $a = 0$ (Schwarzschild case)	18
2. Images for $a = 1/10$ (slowly rotating case)	22
3. Images for $a = 1$ (fast rotating case)	25
4. Images of $G_1$ and emission region of Hawking radiation	28
<b>VI. Summary</b>	29
<b>Acknowledgments</b>	30
<b>References</b>	30

## I. INTRODUCTION

In general relativity, a black hole is defined as the spacetime region surrounded by the event horizon, from which no light signals can escape to the null infinity. There are several possibilities for formation of black holes in our universe; gravitational collapse of stars, coalescence of compact stars, phase transition in the early universe and so on. An important concept characterizing black holes is the photon sphere which is defined as a surface composed of bounded null geodesics [1]. When considering propagation of ingoing null rays towards a black hole, null rays which cross the photon sphere cannot go out of the photon sphere again. This property of the photon sphere predicts an important astrophysical consequence known as black hole shadows. Astrophysical black holes are associated with surrounding gases with light emission. Thus the photon sphere of a black hole can be visible as the rim of a dark shadow region in a bright background emission. Indeed recent observation of the central region of M87 with very large baseline interferometry (VLBI) reported an image of the photon sphere associated with the central supermassive black hole [2–7]. As apparent angular sizes of black hole candidates are very small from the Earth, the key technology to resolve black hole shadows by observation is aperture synthesis; by combining several independent telescopes on the earth, effective size of aperture can be increased and this technique makes it possible to resolve very small apparent sizes of black holes. Image reconstruction of black holes is done based on the property of the wave optics known as

the van Citter-Zernike theorem [8–10], which states that Fourier transformation of the first order degrees of coherence (interferometric fringe pattern) in an observer’s screen provides an intensity distribution of a source object if the spatially incoherence of the source field is assumed.

In this paper, we aim to obtain wave optical images of evaporating black holes. Owing to quantum effect, black holes can emit thermal radiation known as Hawking radiation [11, 12], of which temperature is proportional to the surface gravity of black hole horizons. Hence if we detect Hawking radiation from a spatial far region of a black hole, it is possible to reconstruct wave optical images of the evaporating black hole by applying the van Citter-Zernike theorem. Of course this investigation is just theoretical thought experiment because the Hawking temperatures of astrophysical black holes are too low to detect directly. However, we expect our analysis will provide deeper understanding of Hawking radiation and black hole spacetimes from the viewpoint of the wave optics. Especially, it may be possible to acquire information on the emission region of Hawking radiation by performing wave optical imaging of a black hole, and this direction of investigation is related to the question “where does Hawking radiation originate?” [13, 14]. In our previous works [15, 16], we discussed wave optical imaging of black holes with a coherent point wave source. Interference fringes due to wave scattering by the black hole appear on the observer’s screen. By Fourier transformation of the interference fringe, images of Einstein ring and the photon sphere are obtained. For the evaporating black hole case, wave source is black hole itself and all needed information for imaging is contained in the correlation function of Hawking radiation. Concerning the quantum state of black holes, we assume the Unruh-Hawking vacuum state which is realized as black hole formation via gravitational collapse [1, 11, 12, 17–21]. The vacuum condition is imposed on the past event horizon and the past cosmological horizon of the Kruskal extended Kerr-de Sitter spacetime. For detection of Hawking radiation, we prepare two qubit detectors to measure spatial correlation of Hawking radiation. Then by Fourier transformation of the spatial correlation function, we can obtain wave optical images of black holes.

The plan of this paper is as follows. In Section II, we shortly review the van Citter-Zernike theorem and the qubit detector model. We adopt two qubit detectors as our imaging system which can extract spatial correlation of wave field. In Section III, after reviewing Hawking radiation in the Kerr-de Sitter spacetime, we present the spatial correlation function of Hawking radiation in terms of transmission and reflection coefficients for wave modes. In Section IV, we explain numerical method to evaluate reflection and transmission coefficients. In Section V, we present images of black holes. Section VI is devoted to summary and conclusion. We adopt units  $c = \hbar = G = 1$  throughout this paper.

## II. VAN CITTER-ZERNIKE THEOREM AND WAVE OPTICAL IMAGING

We shortly review a method of wave optical imaging based on the van Citter-Zernike theorem [8–10] and the qubit detector system which is applicable to detect spatial correlations of Hawking radiation to employ image formation based on the van Citter-Zernike theorem.

### A. Van Citter-Zernike theorem

Let us consider emission of scalar wave from a source  $\rho(t, \mathbf{x})$  which possesses random statistical property. We observe the emitted waves far from the source (Fig. 1).

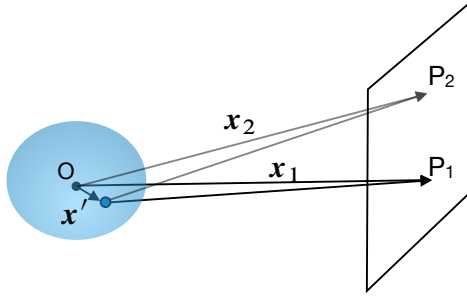


FIG. 1: A wave source is located around the origin. Detection points  $P_1$  and  $P_2$  are assumed to be far from the source.

We consider the scalar wave function  $\Phi$  which obeys a wave equation  $(\partial_t^2 - \nabla^2)\Phi = \rho(t, \mathbf{x})$ . The solution is given by

$$\Phi(t, \mathbf{x}) = \frac{1}{4\pi} \int_{-\infty}^{+\infty} d\omega \int d^3x' \rho_\omega(\mathbf{x}') \frac{e^{-i\omega(t-|\mathbf{x}-\mathbf{x}'|)}}{|\mathbf{x}-\mathbf{x}'|}, \quad (1)$$

where the temporal Fourier transformation of the source field is introduced as

$$\rho(t, \mathbf{x}) = \int_{-\infty}^{+\infty} d\omega e^{-i\omega t} \rho_\omega(\mathbf{x}), \quad \rho_{-\omega} = \rho_\omega^*. \quad (2)$$

As the detection point  $\mathbf{x}$  is far from the source region,  $|\mathbf{x}-\mathbf{x}'| \approx r - \mathbf{x} \cdot \mathbf{x}'/r$  with  $r = |\mathbf{x}|$ . Thus the wave function can be written as

$$\Phi(t, \mathbf{x}) \approx \frac{1}{4\pi r} \int_{-\infty}^{+\infty} d\omega e^{-i\omega(t-r)} \int d^3x' \rho_\omega(\mathbf{x}') e^{-i\omega \mathbf{x} \cdot \mathbf{x}'/r}. \quad (3)$$

The correlation function of the scalar field at  $|\mathbf{x}_1| = |\mathbf{x}_2| = r$  is

$$\begin{aligned} & \langle \Phi(t_1, \mathbf{x}_1) \Phi(t_2, \mathbf{x}_2) \rangle \\ &= \frac{1}{16\pi^2 r^2} \int d\omega_1 d\omega_2 d^3x'_1 d^3x'_2 e^{-i\omega_1(t_1-r) - i\omega_2(t_2-r)} \langle \rho_{\omega_1}(\mathbf{x}'_1) \rho_{\omega_2}(\mathbf{x}'_2) \rangle e^{-i\omega_1(\mathbf{x}_1 \cdot \mathbf{x}'_1)/r - i\omega_2(\mathbf{x}_2 \cdot \mathbf{x}'_2)/r}, \end{aligned} \quad (4)$$

where  $\langle \cdot \rangle$  denotes statistical averaging. We assume stationarity of the source field. Then the correlation of the source depends only on difference of time  $t_1 - t_2$ . In terms of the temporal Fourier component, this property can be expressed as

$$\langle \rho_{\omega_1}(\mathbf{x}'_1) \rho_{\omega_2}(\mathbf{x}'_2) \rangle = I_{\omega_1}(\mathbf{x}'_1, \mathbf{x}'_2) \delta(\omega_1 + \omega_2), \quad I_{\omega}(\mathbf{x}'_1, \mathbf{x}'_2) := \langle \rho_{\omega}(\mathbf{x}'_1) \rho_{\omega}^*(\mathbf{x}'_2) \rangle. \quad (5)$$

Thus

$$\langle \Phi(t_1, \mathbf{x}_1) \Phi(t_2, \mathbf{x}_2) \rangle = \frac{1}{16\pi^2 r^2} \int d\omega d^3 x'_1 d^3 x'_2 e^{-i\omega(t_1-t_2)} I_{\omega}(\mathbf{x}'_1, \mathbf{x}'_2) e^{-i\omega(\mathbf{x}_1 \cdot \mathbf{x}'_1 - \mathbf{x}_2 \cdot \mathbf{x}'_2)/r}. \quad (6)$$

where we have set  $\omega_1 = \omega$  after integrating over  $\omega_2$ . Under the assumption of stationarity of the source, Fourier transformation of the field correlation function is

$$\langle \Phi(t_1, \mathbf{x}_1) \Phi(t_2, \mathbf{x}_2) \rangle = \int_{-\infty}^{+\infty} d\omega e^{-i\omega(t_1-t_2)} G(\omega, \mathbf{x}_1, \mathbf{x}_2), \quad (7)$$

thus the temporal Fourier component of the field correlation becomes

$$G(\omega, \mathbf{x}_1, \mathbf{x}_2) = \frac{1}{16\pi^2 r^2} \int d^3 x'_1 d^3 x'_2 I_{\omega}(\mathbf{x}'_1, \mathbf{x}'_2) e^{-i\omega(\mathbf{x}_1 \cdot \mathbf{x}'_1 - \mathbf{x}_2 \cdot \mathbf{x}'_2)/r}. \quad (8)$$

Now we assume spatial incoherency of the source field which means correlation between different spatial points is zero:

$$I_{\omega}(\mathbf{x}'_1, \mathbf{x}'_2) = I_{\omega}(\mathbf{x}'_1) \delta^3(\mathbf{x}'_1 - \mathbf{x}'_2) \quad (9)$$

with  $I_{\omega}(\mathbf{x}'_1)$  is intensity of the source at  $\mathbf{x}'_1$ . Then

$$\begin{aligned} G(\omega, \mathbf{x}_1, \mathbf{x}_2) &= \frac{1}{16\pi^2 r^2} \int d^3 x' I_{\omega}(\mathbf{x}') e^{-i\omega(\mathbf{x}_1 - \mathbf{x}_2) \cdot \mathbf{x}'/r} \\ &= \frac{1}{16\pi^2 r^2} \int d^2 x'_{\parallel} \tilde{I}_{\omega}(\mathbf{x}'_{\parallel}) e^{-i\omega \mathbf{x}_{12} \cdot \mathbf{x}'_{\parallel}/r} \end{aligned} \quad (10)$$

where we decompose  $\mathbf{x}'$  as  $\mathbf{x}' = \mathbf{x}'_{\perp} + \mathbf{x}'_{\parallel}$ ,  $(\mathbf{x}_1 - \mathbf{x}_2) \cdot \mathbf{x}'_{\perp} = 0$  and  $\mathbf{x}_{12} = \mathbf{x}_1 - \mathbf{x}_2$ . The projected source intensity is introduced by

$$\tilde{I}_{\omega}(\mathbf{x}'_{\parallel}) = \int dx'_{\perp} I_{\omega}(x'_{\perp}, \mathbf{x}'_{\parallel}). \quad (11)$$

After all, we obtain a relation between the spatial field correlation function and the spatial distribution of source intensity

$$G(\omega, \mathbf{x}_1, \mathbf{x}_2) \propto \int d^2 y \tilde{I}_{\omega}(\mathbf{y}) \exp\left(-i\frac{\omega}{r} \mathbf{x}_{12} \cdot \mathbf{y}\right). \quad (12)$$

This formula is called the van Citter-Zernike theorem [8–10]. Thus we can reconstruct distribution of the source intensity (image of the source) from the spatial field correlation function as follows:

$$\tilde{I}_{\omega}(\mathbf{y}) \propto \int d^2 x_{12} G(\omega, \mathbf{x}_1, \mathbf{x}_2) \exp\left(i\frac{\omega}{r} \mathbf{y} \cdot \mathbf{x}_{12}\right). \quad (13)$$

Even if we do not know about property of spatial incoherence of the source,  $\tilde{I}_{\omega}(\mathbf{y})$  obtained by Eq. (13) provides one possible visualization of the source field irrespective of spatial incoherence of the source field.

## B. Qubit detector and response functions

As a measurement apparatus of the spatial correlation of Hawking radiation, we introduce two detectors interacting with Hawking radiation and obtain the field correlation through correlation between two detectors. The detectors are assumed to have two internal levels (qubit) with energy gap  $\omega_0 > 0$ . The interaction Hamiltonian between qubits and the quantum scalar field  $\hat{\Phi}$  (Hawking radiation) is

$$\hat{H}_{\text{int}} = g_1(t)(\sigma_1^+ + \sigma_1^-)\hat{\Phi}(\mathbf{x}_1(t)) + g_2(t)(\sigma_2^+ + \sigma_2^-)\hat{\Phi}(\mathbf{x}_2(t)) \quad (14)$$

where  $\sigma_{1,2}^+, \sigma_{1,2}^-$  are raising and lowering operators for detector's state and  $g_{1,2}(t)$  is a switching function. World lines of detectors are denoted as  $\mathbf{x}_{1,2}(t)$ . This setup of detector system is often employed to investigate entanglement harvesting of quantum fields [22–25]. In our investigation to measure the spatial correlation of the Hawking radiation, two detectors are placed at the same radial coordinate far from the black hole. For the initial ground state of detectors, after interaction with the scalar field, the detector state becomes [25, 26]

$$\rho_{12} = \begin{bmatrix} X_4 & 0 & 0 & X \\ 0 & E_1 & E_{12} & 0 \\ 0 & E_{12} & E_2 & 0 \\ X^* & 0 & 0 & 1 - E_1 - E_2 - X_4 \end{bmatrix}, \quad (15)$$

where

$$X = -2 \int_{-\infty}^{+\infty} dt_1 \int_{-\infty}^{t_1} dt_2 g_1 g_2 e^{i\omega_0(t_1+t_2)} \langle \hat{\Phi}(t_1, \mathbf{x}_1) \hat{\Phi}(t_2, \mathbf{x}_2) \rangle, \quad (16)$$

$$E_{12} = \int_{-\infty}^{+\infty} dt_1 \int_{-\infty}^{+\infty} dt_2 g_1 g_2 e^{-i\omega_0(t_1-t_2)} \langle \hat{\Phi}(t_1, \mathbf{x}_1) \hat{\Phi}(t_2, \mathbf{x}_2) \rangle, \quad (17)$$

$$E_1 = E_{12}|_{2=1}, \quad E_2 = E_{12}|_{1=2}, \quad X_4 = O(g^4). \quad (18)$$

The expectation values of field operators are taken with respect to assumed quantum state of the scalar field. The component  $E_{1,2}(\omega_0)$  represents amount of local quantum fluctuation measured by detectors and shows the Planckian distribution for black hole cases [17, 21]. The component  $X$  represents quantum coherence between two detectors. Actually, entanglement between two detectors can be judged by the entanglement negativity [27] which is proportional to  $|X| - \sqrt{E_1 E_2}$  in the present case. Positive values of this quantity implies two detectors are entangled and entanglement of the quantum field is measured by detectors. Entanglement harvesting in black hole spacetimes is investigated by several papers (BTZ case [24], Schwarzschild case [28], Kerr case [29]). The two point function (Whitman function) is expressed as

$$D^+(t_1, t_2, \mathbf{x}_1, \mathbf{x}_2) := \langle \hat{\Phi}(t_1, \mathbf{x}_1) \hat{\Phi}(t_2, \mathbf{x}_2) \rangle = \int_{-\infty}^{+\infty} d\omega e^{-i\omega(t_1-t_2)} G(\omega, \mathbf{x}_1, \mathbf{x}_2), \quad (19)$$

because of stationarity of the correlation  $D^+(t_1, t_2, \mathbf{x}_1, \mathbf{x}_2) = D^+(t_1-t_2, \mathbf{x}_1, \mathbf{x}_2)$ . By changing integration variables to  $x_1 = (t_1 + t_2)/2$ ,  $y_1 = (t_1 - t_2)/2$  and assuming constant switching

function  $g_1 = g_2 = g$ , we obtain<sup>1</sup>

$$X = -4g^2 \int_{-\infty}^{+\infty} dx e^{2i\omega_0 x} \int_0^{+\infty} dy D^+(2y, \mathbf{x}_1, \mathbf{x}_2) \propto g^2 \delta(\omega_0), \quad (20)$$

$$E_{12} = 2g^2 \int_{-\infty}^{+\infty} dx \int_{-\infty}^{+\infty} dy e^{-2i\omega_0 y} D^+(2y, \mathbf{x}_1, \mathbf{x}_2) = 4\pi g^2 \left( \int dx \right) G(-\omega_0, \mathbf{x}_1, \mathbf{x}_2), \quad (21)$$

$$E_1 = E_{12}|_{\mathbf{x}_2=\mathbf{x}_1}, \quad E_2 = E_{12}|_{\mathbf{x}_1=\mathbf{x}_2}. \quad (22)$$

As  $\omega_0 > 0$ , we have  $X = 0$ . By considering state tomography of the detector system, it is possible to access the component  $E_{12}$  which is proportional to the temporal Fourier component of spatial correlation function  $G(\omega_0, \mathbf{x}_1, \mathbf{x}_2)$ . Therefore, the setup of two detectors can be applicable as an imaging system of black holes with Hawking radiation.

### III. HAWKING RADIATION IN KERR-DE SITTER SPACETIME

We shortly review Hawking radiation in the Kerr-de Sitter spacetime [1, 17–19, 21].

#### A. Basic formulas

We consider a massless conformal scalar field  $\varphi$  in the Kerr-de Sitter (KdS) spacetime. This scalar field is equivalent to the scalar mode of gravitational perturbation which obeys the Teukolsky equation. The metric of the KdS spacetime is

$$ds^2 = -\frac{\Delta_r}{\rho^2 \chi^4} (dt - a \sin^2 \theta d\phi)^2 + \frac{\Delta_\theta}{\rho^2 \chi^4} \sin^2 \theta ((r^2 + a^2)d\phi - a dt)^2 + \rho^2 \left( \frac{dr^2}{\Delta_r} + \frac{d\theta^2}{\Delta_\theta} \right), \quad (23)$$

with

$$\Delta_r = (r^2 + a^2) \left( 1 - \frac{\Lambda}{3} r^2 \right) - 2Mr, \quad \Delta_\theta = 1 + \frac{\Lambda}{3} a^2 \cos^2 \theta, \quad (24)$$

$$\rho^2 = r^2 + a^2 \cos^2 \theta, \quad \chi^2 = 1 + \frac{\Lambda}{3} a^2. \quad (25)$$

Parameters specifying this spacetime are  $(M, a, \Lambda)$ . The scalar field obeys the following wave equation:

$$-\nabla_\mu \nabla^\mu \varphi + \frac{1}{6} R^{(4)} \varphi = 0, \quad (26)$$

where  $R^{(4)}$  is the four dimensional Ricci scalar. We introduce the tortoise coordinate  $r_*$  defined by

$$r_* = \int dr \frac{r^2 + a^2}{\Delta_r} = \frac{\log |r - r_c|}{2\kappa_c} + \frac{\log |r - r_+|}{2\kappa_+} + \frac{\log |r - r_-|}{2\kappa_-} + \frac{\log |r - r_{--}|}{2\kappa_{--}} \quad (27)$$

---

<sup>1</sup>

$$G(-\omega, \mathbf{x}_1, \mathbf{x}_2) = G^*(\omega, \mathbf{x}_1, \mathbf{x}_2), \quad G(-\omega, \mathbf{x}, \mathbf{x}) = G(\omega, \mathbf{x}, \mathbf{x}).$$

where  $r_{--} < 0 < r_- < r_+ < r_c$  are four roots of  $\Delta_r = 0$ ;  $r_+$  is the radius of the outer event horizon and  $r_c$  is the radius of the cosmological horizon (Fig. 2). The surface gravity  $\kappa$  and the angular velocity  $\Omega$  at these points are given by

$$\kappa_j := \kappa(r_j) = \frac{\Delta'_r(r_j)}{2\chi^2(r_j^2 + a^2)}, \quad \Omega_j = \frac{a}{r_j^2 + a^2}, \quad j = --, -, +, c. \quad (28)$$

The right panel of Fig. 2 shows a parameter region for real  $r_+$  and real  $r_c$  in  $(\Lambda M^2, a/M)$  plane [30]. For such values of parameters, we have a Kerr black hole enclosed by a cosmological horizon.

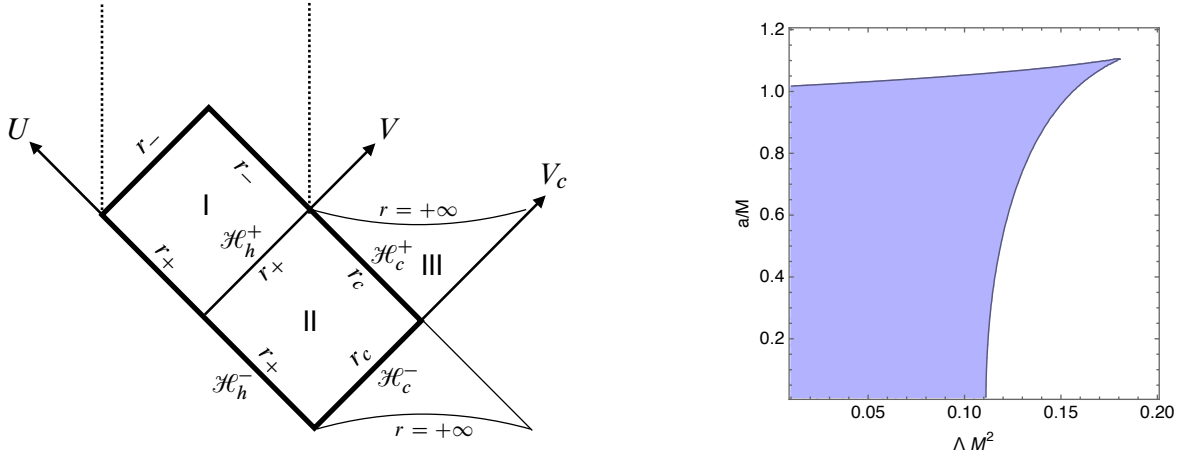


FIG. 2: Left panel: global structure of the KdS spacetime to investigate Hawking radiation with the Unruh-Hawking vacuum state. Dotted vertical lines represent singularity. Right panel: colored region represents parameters for real  $r_+$  and real  $r_c$ . The upper boundary is extremal limit where  $\kappa_+ = 0$ . The lower boundary corresponds to  $r_+ = r_c$  (Nariai limit). Black holes with  $a > 1$  (“over spinning” yet still maintain its horizon structure) are possible for  $\Lambda > 0$ .

The scalar field in the KdS spacetime is separated as

$$\varphi_{\omega\ell m} = \frac{R_{\omega\ell m}(r)}{\sqrt{r^2 + a^2}} S_{\omega\ell m}(\cos\theta) e^{im\phi}, \quad (29)$$

where  $S_{\omega\ell m}(\cos\theta)$  is the angular wave function obeying the following equation:

$$\left[ \frac{d}{d\xi} \{1 + (\chi^2 - 1)\xi^2\} (1 - \xi^2) \frac{d}{d\xi} - 2(\chi^2 - 1)\xi^2 - \frac{\chi^4 \{m - (1 - \xi^2)a\omega\}^2}{\{1 + (\chi^2 - 1)\xi^2\} (1 - \xi^2)} + \lambda_{\ell m}(a\omega, \Lambda) \right] S_{\omega\ell m}(\xi) = 0 \quad (30)$$

with  $\xi = \cos\theta$  and  $\lambda_{\ell m}(a\omega, \Lambda)$  is the eigenvalue of this equation. As the equation (30) has four regular singular points, it can be written in the Heun equation with an appropriate transformation [31, 32] and get the values of  $S_{\omega\ell m}(\xi)$  for the range of  $0 \leq \theta \leq \pi$  using the local Heun functions. Moreover, the eigenvalues  $\lambda_{\ell m}(a\omega, \Lambda)$  are also obtained by finding

the zero point of the Wronskian for the linear independent local Heun functions, which is equivalent to the regularity condition for  $S_{\omega\ell m}(\xi)$  at  $\theta = 0, \pi$  [31, 32]. For the eigenvalues, there is an analytic formula derived in [33]. We have checked that the formula is not so bad even for parameter region  $a\omega \sim O(1)$  with  $\Lambda = 1/100$ , hence we will use the analytic formula in the present paper.

The radial wave function  $R_{\omega\ell m}(r)$  obeys

$$\left[ \frac{d^2}{dr_*^2} - V_{\omega\ell m}(r) \right] R_{\omega\ell m} = 0 \quad (31)$$

with the potential

$$V_{\omega\ell m}(r) = -\chi^4(\omega - m\Omega)^2 + \frac{\Delta_r}{\chi^4(r^2 + a^2)^2} \left\{ \lambda_{\ell m}(a\omega, \Lambda) + \frac{2}{3}\Lambda r^2 + (r^2 + a^2)^{1/2} \left( \frac{r\Delta_r}{(r^2 + a^2)^{3/2}} \right)' \right\}. \quad (32)$$

For the purpose of investigating Hawking radiation, we consider the extended KdS spacetime presented in the left panel of Fig. 2. The Kruskal coordinates about bifurcating horizons  $r_+, r_c$  are defined as

$$U = +\frac{e^{-\kappa_+ u}}{\kappa_+}, \quad V = \frac{e^{\kappa_+ v}}{\kappa_+} \quad \text{in region I,} \quad (33)$$

$$U = -\frac{e^{-\kappa_+ u}}{\kappa_+}, \quad V = \frac{e^{\kappa_+ v}}{\kappa_+}, \quad V_c = -\frac{e^{-\kappa_c v}}{\kappa_c} \quad \text{in region II,} \quad (34)$$

$$V_c = \frac{e^{-\kappa_c v}}{\kappa_c} \quad \text{in region III,} \quad (35)$$

where  $u = t - r_*, v = t + r_*$ .

As the state of Hawking radiation, we adopt the Unruh-Hawking vacuum state which will be defined in the next subsection B. To specify this state, we first introduce the up mode and the dn mode; the mode  $\varphi^{\text{up}}$  has support only in the region II and  $\varphi^{\text{dn}}$  has support only in the region I,<sup>2</sup> and they are defined by imposing their asymptotic forms at the past event horizon as

$$\varphi^{\text{up}}|_{\mathcal{H}_h^-} \sim \exp\left(i\frac{\omega_+}{\kappa_+} \ln(-U)\right) \Theta(-U), \quad \varphi^{\text{dn}}|_{\mathcal{H}_h^-} \sim \exp\left(-i\frac{\omega_+}{\kappa_+} \ln(U)\right) \Theta(U), \quad (36)$$

where  $\Theta(x)$  is the unit step function. Then the UP mode, which is outgoing positive frequency mode with respect to the coordinate  $U$  on the past event horizon  $\mathcal{H}_h^-$ , is defined as a linear combination of  $\varphi^{\text{up}}$  and  $\varphi^{\text{dn}}$  (for  $\omega, \omega_+ > 0$ )

$$\varphi_{\omega_+}^{(\text{UP1})} = \frac{1}{\sqrt{2 \sinh(\pi\omega_+/\kappa_+)}} \left( e^{\pi\omega_+/2\kappa_+} \varphi_{\omega\ell m}^{\text{up}} + e^{-\pi\omega_+/2\kappa_+} (\varphi_{-\omega\ell-m}^{\text{dn}})^* \right), \quad (37)$$

$$\varphi_{-\omega_+}^{(\text{UP2})} = \frac{1}{\sqrt{2 \sinh(\pi\omega_+/\kappa_+)}} \left( e^{\pi\omega_+/2\kappa_+} \varphi_{-\omega\ell-m}^{\text{dn}} + e^{-\pi\omega_+/2\kappa_+} (\varphi_{\omega\ell m}^{\text{up}})^* \right), \quad (38)$$

<sup>2</sup> The modes of the wave equation are normalized with respect to the inner product

$$(\varphi^1, \varphi^2) := i \int_{\Sigma} d\sigma^\mu ((\varphi^1)^* \partial_\mu \varphi^2 - \varphi^2 \partial_\mu (\varphi^1)^*),$$

where  $\Sigma$  is a spacelike or null hypersurface and  $d\sigma^\mu$  is the volume element on this surface.

with  $\omega_+ := \omega - m\Omega_+ > 0$ . The IN mode, which is incoming positive frequency mode with respect to the coordinate  $V_c$  on the past cosmological horizon  $\mathcal{H}_c^-$ , is defined as

$$\varphi_{\omega_c}^{(\text{IN1})} = \frac{1}{\sqrt{2 \sinh(\pi\omega_c/\kappa_c)}} \left( e^{\pi\omega_c/2\kappa_c} \varphi_{\omega}^{\text{in}} + e^{-\pi\omega_c/2\kappa_c} (\varphi_{-\omega}^{\text{ot}})^* \right), \quad (39)$$

$$\varphi_{-\omega_c}^{(\text{IN2})} = \frac{1}{\sqrt{2 \sinh(\pi\omega_c/\kappa_c)}} \left( e^{\pi\omega_c/2\kappa_c} \varphi_{-\omega}^{\text{ot}} + e^{-\pi\omega_c/2\kappa_c} (\varphi_{\omega}^{\text{in}})^* \right), \quad (40)$$

with  $\omega_c := \omega - m\Omega_c$ . The mode  $\varphi_{\omega}^{\text{in}}$  has support only in the region II,  $\varphi_{-\omega}^{\text{ot}}$  has support only in the region III and their asymptotic forms at the past cosmological horizon are specified by

$$\varphi^{\text{in}}|_{\mathcal{H}_c^-} \sim \exp\left(-i\frac{\omega_c}{\kappa_c} \ln(-V_c)\right) \Theta(-V_c), \quad \varphi^{\text{ot}}|_{\mathcal{H}_c^-} \sim \exp\left(i\frac{\omega_c}{\kappa_c} \ln(V_c)\right) \Theta(V_c). \quad (41)$$

The asymptotic behaviors of radial functions  $R_{\omega lm}^{\text{in}} = \sqrt{r^2 + a^2} \varphi_{\omega lm}^{\text{in}}$  and  $R_{\omega lm}^{\text{up}} = \sqrt{r^2 + a^2} \varphi_{\omega lm}^{\text{up}}$  are

$$R_{\omega lm}^{\text{up}} \rightarrow \begin{cases} e^{i\omega_+ r_*} + \tilde{\mathcal{R}}_{\omega lm} e^{-i\omega_+ r_*}, & r_* \rightarrow -\infty \ (r \rightarrow r_+) \\ \tilde{\mathcal{T}}_{\omega lm} e^{i\omega_c r_*}, & r_* \rightarrow +\infty \ (r \rightarrow r_c) \end{cases}, \quad (42)$$

$$R_{\omega lm}^{\text{in}} \rightarrow \begin{cases} \mathcal{T}_{\omega lm} e^{-i\omega_+ r_*}, & r_* \rightarrow -\infty \ (r \rightarrow r_+) \\ e^{-i\omega_c r_*} + \mathcal{R}_{\omega lm} e^{i\omega_c r_*}, & r_* \rightarrow +\infty \ (r \rightarrow r_c) \end{cases}, \quad (43)$$

where reflection coefficients  $\mathcal{R}_{\omega lm}, \tilde{\mathcal{R}}_{\omega lm}$  and transmission coefficients  $\mathcal{T}_{\omega lm}, \tilde{\mathcal{T}}_{\omega lm}$  are introduced. These coefficients satisfy the following relation coming from conservation of the Wronskian:

$$1 - |\mathcal{R}_{\omega lm}|^2 = \frac{\omega_+}{\omega_c} |\mathcal{T}_{\omega lm}|^2, \quad 1 - |\tilde{\mathcal{R}}_{\omega lm}|^2 = \frac{\omega_c}{\omega_+} |\tilde{\mathcal{T}}_{\omega lm}|^2, \quad (44)$$

$$\omega_c \tilde{\mathcal{T}}_{\omega lm}^* \mathcal{R}_{\omega lm} = -\omega_+ \mathcal{T}_{\omega lm} \tilde{\mathcal{R}}_{\omega lm}^*, \quad \omega_c \tilde{\mathcal{T}}_{\omega lm} = \omega_+ \mathcal{T}_{\omega lm}. \quad (45)$$

## B. Correlation function

Introduced combination of modes  $\varphi^{(\text{UP})}, \varphi^{(\text{IN})}$  are called the Unruh modes. Using the Unruh mode functions, the field operator is expanded as

$$\begin{aligned} \hat{\Phi}(x) = & \sum_{\ell m} \int_0^\infty d\omega_+ \left( \hat{a}_{\omega_+}^{(\text{UP1})} \varphi_{\omega_+}^{(\text{UP1})} + \hat{a}_{-\omega_+}^{(\text{UP2})} \varphi_{-\omega_+}^{(\text{UP2})} \right) \\ & + \sum_{\ell m} \int_0^\infty d\omega_c \left( \hat{a}_{\omega_c}^{(\text{IN1})} \varphi_{\omega_c}^{(\text{IN1})} + \hat{a}_{-\omega_c}^{(\text{IN2})} \varphi_{-\omega_c}^{(\text{IN2})} \right) + (\text{h.c.}), \end{aligned} \quad (46)$$

The Unruh-Hawking vacuum state  $|U\rangle$  is defined by

$$\hat{a}_{\omega_+}^{(\text{UP1})} |U\rangle = \hat{a}_{-\omega_+}^{(\text{UP2})} |U\rangle = \hat{a}_{\omega_c}^{(\text{IN1})} |U\rangle = \hat{a}_{-\omega_c}^{(\text{IN2})} |U\rangle = 0, \quad \omega_+, \omega_c \geq 0. \quad (47)$$

This state is realized by black hole formation via gravitational collapse in the KdS spacetime, and the UP mode and the IN mode are thermally populated at the black hole horizon and the

cosmological horizon, respectively. The Hadamard's elementary function with the Unruh-Hawking vacuum state is (we assume  $x_1, x_2 \in$  region II of Fig. 2) <sup>3</sup>

$$\begin{aligned}
G(x_1, x_2) &:= \langle U | \{ \hat{\Phi}(x_1), \hat{\Phi}(x_2) \} | U \rangle \\
&= \sum_{\ell m} \int_0^\infty d\omega_+ \coth\left(\frac{\pi\omega_+}{\kappa_+}\right) \varphi_{\omega\ell m}^{\text{up}}(x_1) \varphi_{\omega\ell m}^{\text{up}*}(x_2) S_{\omega\ell m}(\xi_1) S_{\omega\ell m}(\xi_2) e^{im(\phi_1 - \phi_2)} \\
&\quad + \sum_{\ell m} \int_0^\infty d\omega_c \coth\left(\frac{\pi\omega_c}{\kappa_c}\right) \varphi_{\omega\ell m}^{\text{in}}(x_1) \varphi_{\omega\ell m}^{\text{in}*}(x_2) S_{\omega\ell m}(\xi_1) S_{\omega\ell m}(\xi_2) e^{im(\phi_1 - \phi_2)} + (x_1 \leftrightarrow x_2) + (\text{h.c.}) \\
&= \frac{1}{4\pi(r_1^2 + a^2)^{1/2}(r_2^2 + a^2)^{1/2}} \times \\
&\quad \sum_{\ell m} \int_0^\infty d\omega e^{-i\omega(t_1 - t_2)} \left[ \frac{\Theta(\omega_+)}{\omega_+} \coth\left(\frac{\pi\omega_+}{\kappa_+}\right) R_{\omega\ell m}^{\text{up}}(r_1) R_{\omega\ell m}^{\text{up}*}(r_2) \right. \\
&\quad \left. + \frac{\Theta(\omega_c)}{\omega_c} \coth\left(\frac{\pi\omega_c}{\kappa_c}\right) R_{\omega\ell m}^{\text{in}}(r_1) R_{\omega\ell m}^{\text{in}*}(r_2) \right] S_{\omega\ell m}(\xi_1) S_{\omega\ell m}(\xi_2) e^{im(\phi_1 - \phi_2)} + (1 \leftrightarrow 2) + (\text{h.c.}),
\end{aligned} \tag{48}$$

where  $\xi_{1,2} = \cos\theta_{1,2}$ . To derive the last expression of Eq. (48), we have changed integration variable from  $\omega_+, \omega_c$  to  $\omega$  and introduced the unit step function in the integrant. For  $r_1 = r_2 \rightarrow r_c$ , the temporal Fourier component of the correlation function is given by

$$\begin{aligned}
G(\omega, \mathbf{x}_1, \mathbf{x}_2) &\propto \sum_{\ell m} \left[ \frac{\Theta(\omega_+)}{\omega_+} \coth\left(\frac{\pi\omega_+}{\kappa_+}\right) |\tilde{\mathcal{T}}_{\omega\ell m}|^2 \right. \\
&\quad \left. + \frac{\Theta(\omega_c)}{\omega_c} \coth\left(\frac{\pi\omega_c}{\kappa_c}\right) |1 + \mathcal{R}_{\omega\ell m} e^{i\delta}|^2 \right] S_{\omega\ell m}(\xi_1) S_{\omega\ell m}(\xi_2) e^{im(\phi_1 - \phi_2)} \\
&\equiv G_1 + G_2,
\end{aligned} \tag{49}$$

where a phase factor  $\delta = 2\omega_c r_*$  is introduced. As the radial function  $R^{\text{in}}$  is a liner combination of the incoming wave and the reflected wave with amplitude  $\mathcal{R}_{\omega\ell m}$ ,  $G_2$  contains phase information determined by the reflection coefficient and  $\delta$ . Coefficients  $\coth(\pi\omega_+/\kappa_+)$  and  $\coth(\pi\omega_c/\kappa_c)$  reflect thermal property of the black hole horizon and the cosmological horizon, respectively. For  $\omega_+ \rightarrow 0$ ,  $|\tilde{\mathcal{T}}_{\omega\ell m}| \rightarrow \omega_+$  (see Eq. (45)) and  $G_1(\omega)$  is finite, whereas  $G_2$  diverges for  $\omega_c \rightarrow 0$ .

The Fourier component of Hadamard's elementary function  $G$  consists of contribution  $G_1$  of the up mode and  $G_2$  of the in mode.  $G_1$  represents illumination of the black hole by both the thermally populated UP mode with the Hawking temperature  $\kappa_+/2\pi$  and vacuum fluctuation from inside of the photon sphere. On the other hand,  $G_2$  contains contribution of the IN mode and represents scattering of the incoming thermal radiation with temperature  $\kappa_c/2\pi$  from the cosmological horizon and the vacuum fluctuation by the black hole. These radiations illuminate the black hole from outside of the photon sphere. Concerning the superradiant phenomena,  $G_1$  includes no superradiant modes because it only contains  $\omega_+ > 0$

<sup>3</sup>  $(u_\omega(r))^* = u_{-\omega}(r)$ .

modes, whereas  $G_2$  includes superradiant modes  $\omega_+ < 0 < \omega_c$  and has a chance of superradiant scattering effect.

In  $G_2$ , the phase factor coming from the reflection coefficient  $\mathcal{R}_{\omega\ell m}e^{i\delta}$  provides the interference term between the incoming wave and the reflected wave. As behavior of the interference term depends on  $r_*$ , and for the purpose of qualitative understanding of images of the black hole, it is convenient to evaluate  $G_2$  by replacing  $|1 + \mathcal{R}_{\omega\ell m}e^{i\delta}|^2$  to  $1 + |\mathcal{R}_{\omega\ell m}|^2$  which corresponds to dropping the interference term between the incoming waves and the reflected waves. For this purpose, we introduce the correlation function without the interference term as

$$\tilde{G}_2 := \sum_{\ell m} \frac{\Theta(\omega_c)}{\omega_c} \coth\left(\frac{\pi\omega_c}{\kappa_c}\right) \left(2 - \frac{\omega_c}{\omega_+} |\tilde{\mathcal{T}}_{\omega\ell m}|^2\right) S_{\omega\ell m}(\xi_1) S_{\omega\ell m}(\xi_2) e^{im(\phi_1 - \phi_2)}, \quad (50)$$

where we used the relation (44) and (45) to express  $|\mathcal{R}_{\omega\ell m}|^2$  using  $|\tilde{\mathcal{T}}_{\omega\ell m}|^2$ . The correlation function  $G = G_1 + \tilde{G}_2$  neglects the interference term between incoming waves and reflected waves.

To extract pure thermal effect of Hawking radiation, we write down  $G(\omega)$  for the Boulware vacuum which includes no thermal emission from the black hole horizon and the cosmological horizons. The form of the correlation function for this vacuum state formally obtained by taking limit of  $\kappa_+ \rightarrow 0, \kappa_c \rightarrow 0$  in (49):

$$\begin{aligned} G^{\text{Boulware}}(\omega) & \propto \sum_{\ell m} \left[ \frac{\Theta(\omega_+)}{\omega_+} |\tilde{\mathcal{T}}_{\omega\ell m}|^2 + \frac{\Theta(\omega_c)}{\omega_c} |1 + \mathcal{R}_{\omega\ell m}e^{i\delta}|^2 \right] S_{\omega\ell m}(\xi_1) S_{\omega\ell m}(\xi_2) e^{im(\phi_1 - \phi_2)} \\ & = \sum_{\ell m} \left[ \frac{\Theta(\omega_+)}{\omega_c} (2 + 2\text{Re}[\mathcal{R}_{\omega\ell m}e^{i\delta}]) + \frac{\Theta(-\omega_+)}{\omega_c} |1 + \mathcal{R}_{\omega\ell m}e^{i\delta}|^2 \right] S_{\omega\ell m}(\xi_1) S_{\omega\ell m}(\xi_2) e^{im(\phi_1 - \phi_2)}, \end{aligned} \quad (51)$$

where we assume there are no superradiant modes associated with the cosmological horizon ( $\omega_c > 0$ ). The contribution of particle creations from the black hole and the cosmological horizon in the correlation function is encoded in the following two point function obtained by subtracting contribution of the Boulware vacuum and this correlation function includes the Planckian factor:

$$\begin{aligned} G(\omega) - G^{\text{Boulware}}(\omega) & \propto \sum_{\ell m} \left[ \frac{\Theta(\omega_+)}{e^{2\pi\omega_+/\kappa_+} - 1} \frac{|\tilde{\mathcal{T}}_{\omega\ell m}|^2}{\omega_+} + \frac{\Theta(\omega_c)}{e^{2\pi\omega_c/\kappa_c} - 1} \frac{|1 + \mathcal{R}_{\omega\ell m}e^{i\delta}|^2}{\omega_c} \right] S_{\omega\ell m}(\xi_1) S_{\omega\ell m}(\xi_2) e^{im(\phi_1 - \phi_2)}. \end{aligned} \quad (52)$$

By its definition,  $G - G^{\text{Boulware}}$  becomes zero for  $\kappa_+, \kappa_c \rightarrow 0$ . We use this correlation function for images of the black hole which reflect directly the Hawking effect.

#### IV. EVALUATION OF TRANSMISSION AND REFLECTION COEFFICIENTS

In this section, we introduce our computation of the greybody factor  $|\tilde{\mathcal{T}}_{\omega\ell m}|^2$  and the reflection coefficient  $\mathcal{R}_{\omega\ell m}$ . We adopt the method developed in [32], which utilizes the local solutions around regular singular points of the Heun equation (local Heun function) with the Frobenius method to construct solutions of the Teukolsky equation. The local Heun functions have been implemented as built-in functions in Mathematica version 12.1 updated in 2020. We comment here the relation between scattering problems based on the Teukolsky radial function  $R^{(T)}$  and on the radial function  $R$  introduced by (29). They are related as  $R^{(T)} = R/\sqrt{r^2 + a^2}$ .  $R^{(T)}$  obeys

$$\left[ \frac{d}{dr} \Delta_r \frac{d}{dr} + \frac{\chi^4}{\Delta_r} [\omega(r^2 + a^2) - am]^2 - \frac{2\Lambda}{3} r^2 - \lambda_{\ell m}(a\omega, \Lambda) \right] R^{(T)} = 0. \quad (53)$$

This equation is same as that of the massless conformal scalar field in the KdS spacetime. To use the method with the local Heun function, we transform the above equation into the Heun equation by introducing the coordinate transformation from  $r$  to  $z$  and the redefinition of the radial equation as follows:

$$z = \frac{r_c - r_-}{r_c - r_+} \frac{r - r_+}{r - r_-}, \quad R^{(T)} = z^{B_1} (z - 1)^{B_2} (z - z_r)^{B_3} (z - z_\infty) y^{(r)}(z), \quad (54)$$

and the radial equation yields

$$\frac{d^2 y^{(r)}}{dz^2} + \left( \frac{2B_1 + 1}{z} + \frac{2B_2 + 1}{z - 1} + \frac{2B_3 + 1}{z - z_r} \right) \frac{dy^{(r)}}{dz} + \frac{(1 - 2B_4)z + v}{z(z - 1)(z - z_r)} y^{(r)} = 0, \quad (55)$$

where

$$z_\infty = \frac{r_c - r_-}{r_c - r_+}, \quad z_r = z_\infty \frac{r_{--} - r_+}{r_{--} - r_-}, \quad B_j = i \frac{\chi^2 (r_j^2 + a^2) (\omega - m\Omega_j)}{\Delta'_r(r_j)}, \quad (56)$$

with  $B_1 = B_+$ ,  $B_2 = B_c$ ,  $B_3 = B_{--}$ ,  $B_4 = B_-$  and

$$v = \frac{\lambda_{\ell m} - (\Lambda/3)(r_+ r_- + r_c r_{--})}{(\Lambda/3)(r_- - r_{--})(r_+ - r_c)} - \frac{i[2\chi^2\{\omega(r_+ r_- + a^2) - am\}]}{(\Lambda/3)(r_- - r_{--})(r_- - r_+)(r_+ - r_c)}. \quad (57)$$

The sets of the linear independent local solutions of equation (55) at  $z = 0$  (black hole outer horizon) and at  $z = 1$  (cosmological horizon) are represented as  $(y_{01}, y_{02})$  and  $(y_{11}, y_{12})$ , respectively [32]. These solutions are related to each other as

$$y_{01}(z) = C_{11} y_{11}(z) + C_{12} y_{12}(z), \quad y_{02}(z) = C_{21} y_{11}(z) + C_{22} y_{12}(z), \quad (58)$$

$$y_{11}(z) = D_{11} y_{01}(z) + D_{12} y_{02}(z), \quad y_{12}(z) = D_{21} y_{01}(z) + D_{22} y_{02}(z), \quad (59)$$

with the connection coefficients

$$C_{11} = \frac{W_z[y_{01}, y_{12}]}{W_z[y_{11}, y_{12}]}, \quad C_{12} = \frac{W_z[y_{01}, y_{11}]}{W_z[y_{12}, y_{11}]}, \quad C_{21} = \frac{W_z[y_{02}, y_{12}]}{W_z[y_{11}, y_{12}]}, \quad C_{22} = \frac{W_z[y_{02}, y_{11}]}{W_z[y_{12}, y_{11}]}, \quad (60)$$

and

$$D_{11} = \frac{W_z[y_{11}, y_{02}]}{W_z[y_{01}, y_{02}]}, \quad D_{12} = \frac{W_z[y_{11}, y_{01}]}{W_z[y_{02}, y_{01}]}, \quad D_{21} = \frac{W_z[y_{12}, y_{02}]}{W_z[y_{01}, y_{02}]}, \quad D_{22} = \frac{W_z[y_{12}, y_{01}]}{W_z[y_{02}, y_{01}]}, \quad (61)$$

where  $W_z[u, v] = u(dv/dz) - v(du/dz)$ . Note that the local solutions are evaluated with the build-in function `HeunG` in `Mathematica`<sup>4</sup>.

To obtain the greybody factor and the reflection coefficient, we investigate the behavior of the in and up modes in terms of  $R(r_*)$  and  $R^T(r)$ . In the tortoise coordinate  $r_*$ , up and in modes have been obtained as Eqs. (42) and (43). Equivalently, in the  $r$  coordinate, it becomes

$$R^{(T)\text{up}} \rightarrow \begin{cases} D^{(\text{up})} \Delta_r^{B_1} + D^{(\text{ref})} \Delta_r^{-B_1}, & r \rightarrow r_+ \\ D^{(\text{trans})} \Delta_r^{B_2}, & r \rightarrow r_c \end{cases} \quad (62)$$

$$R^{(T)\text{in}} \rightarrow \begin{cases} C^{(\text{trans})} \Delta_r^{-B_1}, & r \rightarrow r_+ \\ C^{(\text{ref})} \Delta_r^{B_2} + C^{(\text{inc})} \Delta_r^{-B_2}, & r \rightarrow r_c. \end{cases} \quad (63)$$

The reflection coefficient  $\mathcal{R}_{\omega\ell m}$  and the greybody factor  $|\tilde{\mathcal{T}}_{\omega\ell m}|^2$  can be written with the coefficients of the above solutions as

$$\mathcal{R}_{\omega\ell m} = \frac{C^{(\text{ref})}}{C^{(\text{inc})}}, \quad |\tilde{\mathcal{T}}_{\omega\ell m}|^2 = \left( \frac{r_c^2 + a^2}{r_+^2 + a^2} \right) \left| \frac{D^{(\text{trans})}}{D^{(\text{up})}} \right|^2 \quad (64)$$

by comparing the asymptotic form of  $R(r_*)$  and  $R^T(r)$  using the relation between  $r_*$  and  $r$ . Furthermore,  $C^{(\text{ref/up/trans})}$  and  $D^{(\text{ref/up/trans})}$  are represented with the connection coefficients of the local Heun functions as demonstrated by [32] as

$$C^{(\text{inc})} = C_{22}(-1)^{B_2}(1-z_r)^{B_3}(1-z_\infty)(A_2)^{-B_2}, \quad (65)$$

$$\begin{aligned} C^{(\text{ref})} &= C_{21}D^{(\text{trans})} \\ &= C_{21}(-1)^{B_2}(1-z_r)^{B_3}(1-z_\infty)(A_2)^{B_2}, \end{aligned} \quad (66)$$

$$D^{(\text{up})} = D_{11}(-1)^{B_2}(-z_r)^{B_3}(-z_\infty)(A_1)^{B_1}, \quad (67)$$

$$\begin{aligned} D^{(\text{ref})} &= D_{12}C^{(\text{trans})} \\ &= D_{12}(-1)^{B_2}(-z_r)^{B_3}(-z_\infty)(A_1)^{-B_1}, \end{aligned} \quad (68)$$

with

$$A_1 = \frac{z_\infty}{(r_+ - r_-)\Delta'(r_+)}, \quad A_2 = \frac{z_\infty(r_+ - r_-)}{-(r_c - r_-)^2\Delta'(r_c)}. \quad (69)$$

<sup>4</sup> See the detailed computation in [32].

## V. IMAGING OF BLACK HOLES WITH HAWKING RADIATION

As we have shown in Eq. (21), the qubit detectors system is applicable to detect the spatial correlation of Hawking radiation and we adopt it as our imaging system for black holes.

### A. Detail of imaging method and an example with a simple model

In our setup of imaging, two detectors are placed near the cosmological horizon. In the spherical coordinates system, the detector 1 is placed at  $(r, \theta_1, \phi_1) = (r, \pi/2, 0)$  (on the equatorial plane) and the detector 2 is placed at  $(r, \theta_2, \phi_2)$ . In the Cartesian coordinates  $(x, y, z) = (r \sin \theta \cos \phi, r \sin \theta \sin \phi, r \cos \theta)$ , detectors locations are

$$\mathbf{x}_1 = (r, 0, 0), \quad \mathbf{x}_2 = (r \sin \theta \cos \phi, r \sin \theta \sin \phi, r \cos \theta). \quad (70)$$

We define two dimensional coordinates in the observer's screen as

$$\mathbf{X} = (X, Y) = (\sin \theta \sin \phi, \cos \theta). \quad (71)$$

Then the locations of two detectors in the observer's screen are

$$(X_1, Y_1) = (0, 0) = \mathbf{X}_1, \quad (X_2, Y_2) = (\sin \theta \sin \phi, \cos \theta) = \mathbf{X}_2, \quad (72)$$

Applying Eq. (13), images (intensity distributions) are obtained by the following Fourier transformation of the correlation function in the observer's screen:

$$\mathcal{F}[G](\mathbf{X}_{\text{im}}) := \int d^2 \mathbf{X}_{12} G(\omega, \mathbf{X}_1, \mathbf{X}_2) \exp(i\omega \mathbf{X}_{\text{im}} \cdot \mathbf{X}_{12}), \quad \mathbf{X}_{12} = \mathbf{X}_1 - \mathbf{X}_2, \quad (73)$$

where  $\mathbf{X}_{\text{im}}$  denotes coordinates in the image plane.

To check our imaging method, we present analytic evaluation of images for the following model correlation function  $G = G_1 + \tilde{G}_2$  which includes important features of the correlation function coming from Hawking radiation of the Schwarzschild black hole:

$$G_1 = \frac{g_1}{\omega} \sum_{\ell=0}^{\infty} \Theta(\ell_* - \ell) (2\ell + 1) P_\ell(\cos \Delta), \quad \tilde{G}_2 = \frac{g_2}{\omega} \sum_{\ell=0}^{\infty} (1 + \Theta(\ell - \ell_*)) (2\ell + 1) P_\ell(\cos \Delta), \quad (74)$$

where transmission and reflection coefficients are replaced with the unit step function which reflect the property of perfect absorption of black holes. The parameter  $\ell_*$  denotes the critical angular momentum of perfect absorption corresponding to the photon sphere and  $\Delta := \theta - \pi/2$  is the angle between an observing point and the optical axis. This model well represents the correlation function of Hawking radiation in the eikonal region.  $g_1, g_2$  are constants of which values depend on surface gravity of horizons

$$g_1 = \coth\left(\frac{\pi\omega}{\kappa_+}\right), \quad g_2 = \coth\left(\frac{\pi\omega}{\kappa_c}\right). \quad (75)$$

By replacing the sum with integral, it is possible to evaluate the correlation function analytically; with approximation  $P_\ell(\cos \Delta) \sim J_0(\ell\Delta)$ ,  $\ell \gg 1$  and replacing upper bound of the infinite sum by  $\ell_{\text{max}} \gg \ell_*$ , we obtain

$$G_1 \approx \frac{2g_1}{\omega} \int_0^{\ell_*} d\lambda \lambda P_\lambda(\cos \Delta) = \frac{2g_1}{\omega} \int_0^{\ell_*} d\lambda \lambda J_0(\lambda\Delta) = \frac{2g_1 \ell_*}{\omega \Delta} J_1(\ell_* \Delta), \quad (76)$$

and

$$\begin{aligned}\tilde{G}_2 &= \frac{g_2}{\omega} \sum_{\ell=0}^{\ell_{\max}} (2\ell+1) P_\ell(\cos \Delta) + \frac{g_2}{\omega} \left( \sum_{\ell=0}^{\ell_{\max}} - \sum_{\ell=0}^{\ell_*} \right) (2\ell+1) P_\ell(\cos \Delta) \\ &\approx \frac{4g_2}{\omega} \frac{\ell_{\max}}{\Delta} J_1(\ell_{\max}\Delta) - \frac{2g_2}{\omega} \frac{\ell_*}{\Delta} J_1(\ell_*\Delta).\end{aligned}\quad (77)$$

The angle  $\Delta$  is related to coordinates  $(X, Y)$  in the observer's screen as  $\Delta = \sqrt{X^2 + Y^2} < 1$ .

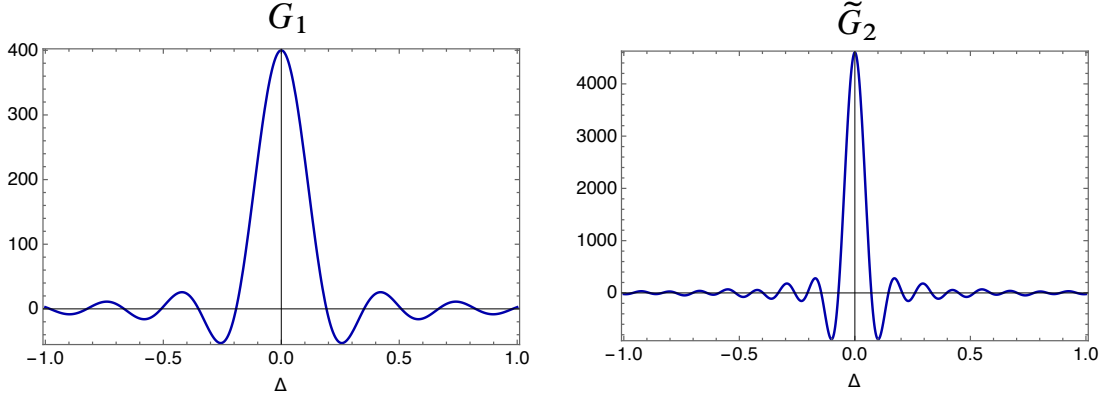


FIG. 3:  $G_1, \tilde{G}_2$  with  $\ell_* = 20, \ell_{\max} = 50, \omega = 1, g_1 = g_2 = 1$ .

Figure 3 shows behavior of  $G_1, \tilde{G}_2$ .  $G_1$  represents interference fringe due to Hawking radiation from the black hole. For  $\ell_{\max} \rightarrow \infty$ , the peak of  $\tilde{G}_2$  at  $\Delta = 0$  becomes infinite and the peak approaches the Dirac delta function.

Now we consider two dimensional Fourier transformation (73) of a function  $f(\sqrt{X^2 + Y^2})$

$$\mathcal{F}[f] = \frac{1}{2\pi} \int_{-\infty}^{+\infty} dX dY f(\sqrt{X^2 + Y^2}) e^{i\omega(X_{\text{im}}X + Y_{\text{im}}Y)}, \quad (78)$$

where  $X_{\text{im}}, Y_{\text{m}}$  are coordinates in the image plane. Then

$$\begin{aligned}\mathcal{F}[f] &= \frac{1}{2\pi} \int dX dY f(\sqrt{X^2 + Y^2}) e^{i\omega(X_{\text{im}}X + Y_{\text{im}}Y)} \\ &= \frac{1}{2\pi} \int_0^\infty \Delta(d\Delta) \int_0^{2\pi} d\phi f(\Delta) e^{i\omega\sqrt{X_{\text{im}}^2 + Y_{\text{im}}^2} \Delta \cos \phi} \\ &= \int_0^\infty \Delta(d\Delta) J_0(\omega R_{\text{im}}\Delta) f(\Delta),\end{aligned}\quad (79)$$

where  $R_{\text{im}} := \sqrt{X_{\text{im}}^2 + Y_{\text{im}}^2}$ . Applying this formula<sup>5</sup>, we obtain

$$\mathcal{F}[G_1] \propto \frac{2g_1}{\omega} \Theta(\ell_*/\omega - R_{\text{im}}), \quad (80)$$

$$\mathcal{F}[\tilde{G}_2] \propto \frac{4g_2}{\omega} \Theta(\ell_{\text{max}}/\omega - R_{\text{im}}) - \frac{2g_2}{\omega} \Theta(\ell_*/\omega - R_{\text{im}}), \quad (81)$$

$$\mathcal{F}[G_1 + \tilde{G}_2] \propto \frac{4g_2}{\omega} \Theta(\ell_{\text{max}}/\omega - R_{\text{im}}) - \frac{2g_2 - 2g_1}{\omega} \Theta(\ell_*/\omega - R_{\text{im}}). \quad (82)$$

Figure 4 shows images obtained from the correlation function (74).

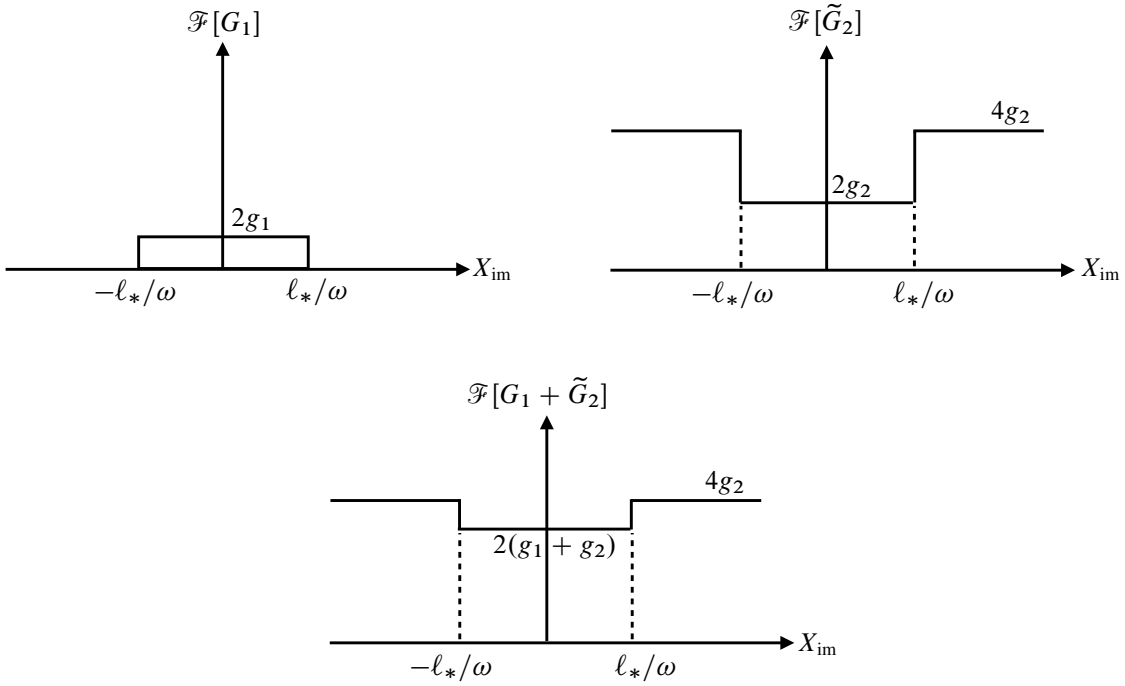


FIG. 4: One dimensional images obtained from the correlation function (74). The lower panel is  $\mathcal{F}[G_1 + \tilde{G}_2]$  for  $\kappa_c > \kappa_+$  case for low frequency.

For high frequency region  $\omega > \kappa_{+,c}/(2\pi)$ ,  $g_1 \approx g_2 \approx 1$  holds and  $\mathcal{F}[G_1 + \tilde{G}_2]$  becomes constant which means images  $\mathcal{F}[G_1]$  and  $\mathcal{F}[\tilde{G}_2]$  are complement each other. On the other hand for low frequency region  $\omega < \kappa_{+,c}/(2\pi)$ ,  $g_1 \approx \kappa_+/(2\pi\omega)$ ,  $g_2 \approx \kappa_c/(2\pi\omega)$ . Thus for  $\kappa_+ < \kappa_c$ , emission from the cosmological horizon has higher temperature and the image  $\mathcal{F}[G_1 + \tilde{G}_2]$  shows dark region with radius  $\ell_*/\omega$  which corresponds to the black hole shadow. On the contrary for  $\kappa_+ > \kappa_c$ , the image  $\mathcal{F}[G_1 + \tilde{G}_2]$  shows a bright disk which represents emission of Hawking radiation from the black hole.

<sup>5</sup>

$$\int_0^\infty dx J_0(ax) J_1(bx) = \frac{1}{b} \Theta(b - a).$$

## B. Black hole images

Now, we move on to the image reconstruction of black holes using Eqs. (49) and (52). Assumption of detector 1's position on the equatorial plane reduces much computational time because in the summation with respect to  $\ell, m$  of  $G_1, G_2$ , the spheroidal harmonics  $S_{\omega\ell m}(\pi/2, 0)$  is nonzero only for  $m = \ell, \ell - 2, \dots, -(\ell - 2), -\ell$ . To evaluate  $G_2$ , we must truncate infinite sum of  $\ell$  with sufficiently large value  $\ell_{\max}$  which does not change qualitative behavior of the correlation function. A rough estimation to determine  $\ell_{\max}$  is as follows; for the radial distance of observation  $r_{\text{obs}}$ ,  $\ell_{\max}$  is estimated as  $r_{\text{obs}} \sim \ell_{\max}/\omega$ . Thus  $\ell_{\max} \gtrsim \omega r_{\text{obs}}$  is required. In our calculation, we choose  $\ell_{\max} = 70$  for  $\omega = 5$  and  $\ell_{\max} = 7$  for  $\omega = 0.5$ . These values are chosen as larger than the value of  $\ell$  corresponding to photon sphere of the black hole. The original correlation function Eq. (48) includes the prefactor  $1/(4\pi(r_{\text{obs}}^2 + a^2))$  which depends on  $r_{\text{obs}}$ . This factor only affects total intensity of images and the structure of images is not altered if we omit this factor.  $G_2$  contains  $r_{\text{obs}}$  as the phase factor  $\delta = 2\omega_c r_*|_{\text{obs}}$ . In our analysis, we does not fix  $r_{\text{obs}}$  and  $\delta$  is chosen as  $0, \pi/2, \pi, 3\pi/2$ . As for the black hole parameters, we choose  $a = 0, 0.1, 1$  and  $\Lambda = 1/100$ . For these values, horizon radius and surface gravity are (in unit of  $M = 1$ )

$$\begin{aligned}
 a = 0 : & \quad r_+ = 2.028, \quad r_c = 16.22, \quad \kappa_+ = 0.2364, \quad \kappa_c = 0.05026, \\
 a = 0.1 : & \quad r_+ = 2.023, \quad r_c = 16.22, \quad \kappa_+ = 0.2359, \quad \kappa_c = 0.05025, \\
 a = 1 : & \quad r_+ = 1.094, \quad r_c = 16.22, \quad \kappa_+ = 0.03685, \quad \kappa_c = 0.05015.
 \end{aligned} \tag{83}$$

In the observer's screen, we evaluate  $G_1, G_2$  in a region  $-1 \leq \theta - \pi/2 \leq 1, -1 \leq \phi \leq 1$  with  $60 \times 60$  sampling points by taking summation with respect to  $\ell, m$ . In our calculation of images, we pick up data points of  $X^2 + Y^2 < 1/4$  in the observer's screen which defines the aperture of our imaging system. We applied the Tukey window to reduce unwanted aliasing comes from sharp cutoff of the aperture in discrete Fourier transformation in a finite region. Around the equatorial plane  $\theta \approx \pi/2$ , difference between the spheroidal harmonics  $S_{\omega\ell m}$  and the spherical harmonics  $Y_{\ell m}$  is not so large; indeed, the relative difference of them is smaller than 0.1 even for  $\ell \geq 5$  with  $a\omega = 5$  case. Thus we evaluate the sum in  $G$  by replacing  $S_{\omega\ell m}$  with  $Y_{\ell m}$  to reduce computational time. We checked relative difference of  $G$  is less than 1 % for  $a\omega = 5$  case, hence we expect this replacement does not produce much qualitative difference of images.

### 1. Images for $a = 0$ (Schwarzschild case)

Figure 5 shows reflection and transmission coefficients in  $(\ell, m)$ -plane and  $G_1, G_2$  for  $\omega = 5$ . As the black hole is spherically symmetric, reflection and transmission coefficients has no  $m$  dependence. Dependence of  $\ell$  of the reflection coefficient contains information of the phase shift of waves scattered by the black hole. For  $\ell \leq \ell_* \approx 25$ ,  $\mathcal{R}_{\omega\ell m} \sim 0, \tilde{\mathcal{T}}_{\omega\ell m} \sim 1$  and incoming waves from spatial infinity are perfectly absorbed by the black hole. This critical value  $\ell_*/\omega \sim 5M$  corresponds to the size of photon sphere of the Schwarzschild black hole. Behavior of  $|\mathcal{R}_{\omega\ell m}|$  and  $|\tilde{\mathcal{T}}_{\omega\ell m}|$  show conservation law  $|\mathcal{R}_{\omega\ell m}|^2 + |\tilde{\mathcal{T}}_{\omega\ell m}|^2 = 1$ . Correlation functions  $G_1, G_2$  on the observer's screen show circular interference fringes.  $G_2$  has a sharp peak at the origin which is originated by the incoming radiation from the cosmological horizon. Fourier transformation of this peak provides nearly homogeneous background intensity of images. Imaginary part of  $G$  is zero for  $a = 0$  case.

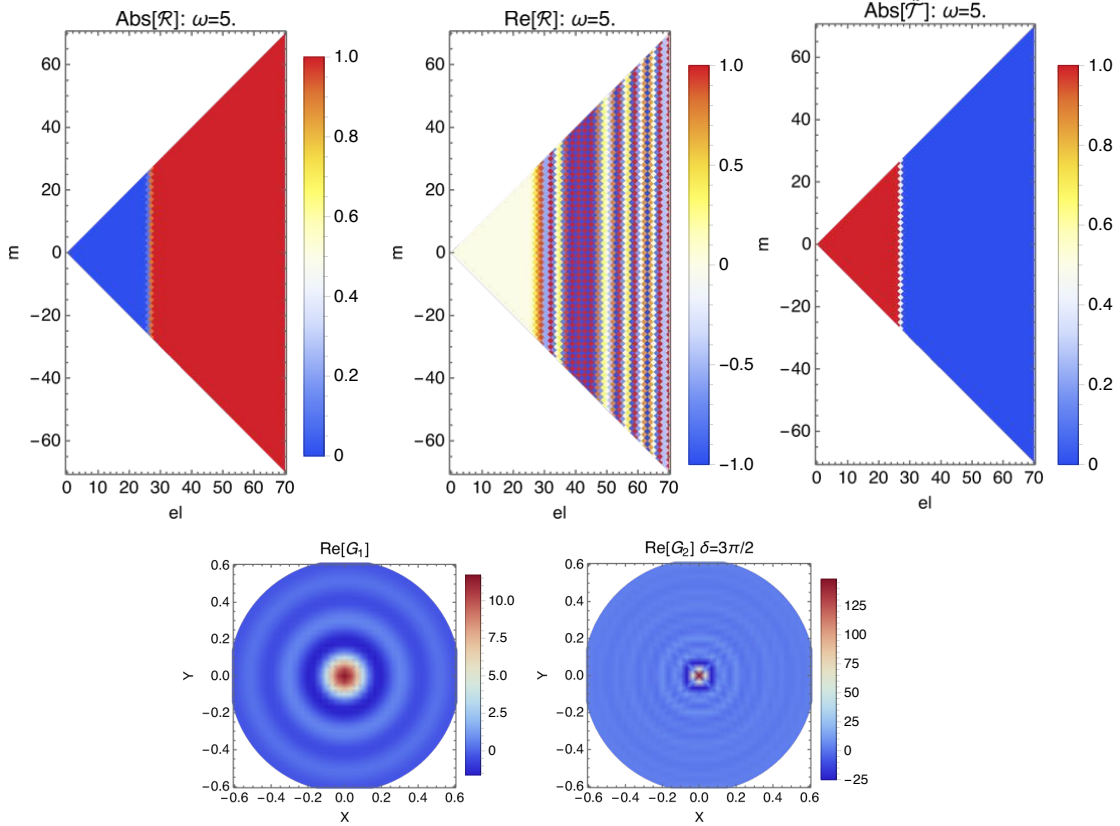


FIG. 5: Reflection and transmission coefficients in  $(\ell, m)$ -plane (upper panels) and  $G_1, G_2$  on the observer's screen (lower panels) for  $a = 0$  with  $\omega = 5$ .  $G_1$  shows interference fringes caused by Hawking radiation emitted by the black hole.  $G_2$  shows interference fringes caused by scattering of incoming radiation from the cosmological horizon by the black hole. A sharp peak in  $G_2$  at  $X = Y = 0$  is due to the background incoming mode from the cosmological horizon, which results in homogeneous background intensity distribution in images. Imaginary part of  $G_{1,2}$  is zero.

Figure 6 shows images obtained by Fourier transformation of  $G$ .  $\mathcal{F}[G_1]$  is the image of the black hole by the UP mode with the vacuum fluctuation. We superimpose the photon sphere (dotted circle) with the image. As the photon sphere is concept in geometric optics, its shape has a finite width in wave optics. To identify the location of the photon sphere in our calculation, we define it as the location where intensity of  $\mathcal{F}[G_1]$  becomes one-half compared to that of the central bright region. The black hole looks like a “shining star” with its surface coincides with the photon sphere.  $\mathcal{F}[G_2]$  and  $\mathcal{F}[\tilde{G}_2]$  are images of black hole illuminated by the IN mode which is incoming radiation from the cosmological horizon. The emission from the black hole is not included in  $G_2$  and  $\tilde{G}_2$ . The incoming radiation is scattered and absorbed by the black hole. A dark circular shadow region surrounded by a bright ring appears in these images. The shadow region is not black because  $G_2$  has a contribution of incoming waves directly reaches detectors from the cosmological horizon (see Fig. 4).  $\mathcal{F}[G_1 + G_2]$  and  $\mathcal{F}[G_1 + \tilde{G}_2]$  are images with contributions of both the UP mode and the IN mode. The black hole is visible as a bright disk in  $\mathcal{F}[G_1 + G_2]$ . Comparing these two images, interference effect sharpen the structure of the photon sphere. We can confirm this behavior more clearly by checking one dimensional slice of the images (right panels of Fig. 6.

Slices of images along  $Y_{\text{im}} = 0$  line). Depending on values of the phase  $\delta$ , intensity around the photon sphere becomes brighter and darker compared to the image without interference effect. Intensity of inside and outside of the photon sphere is not affected by values of  $\delta$ .

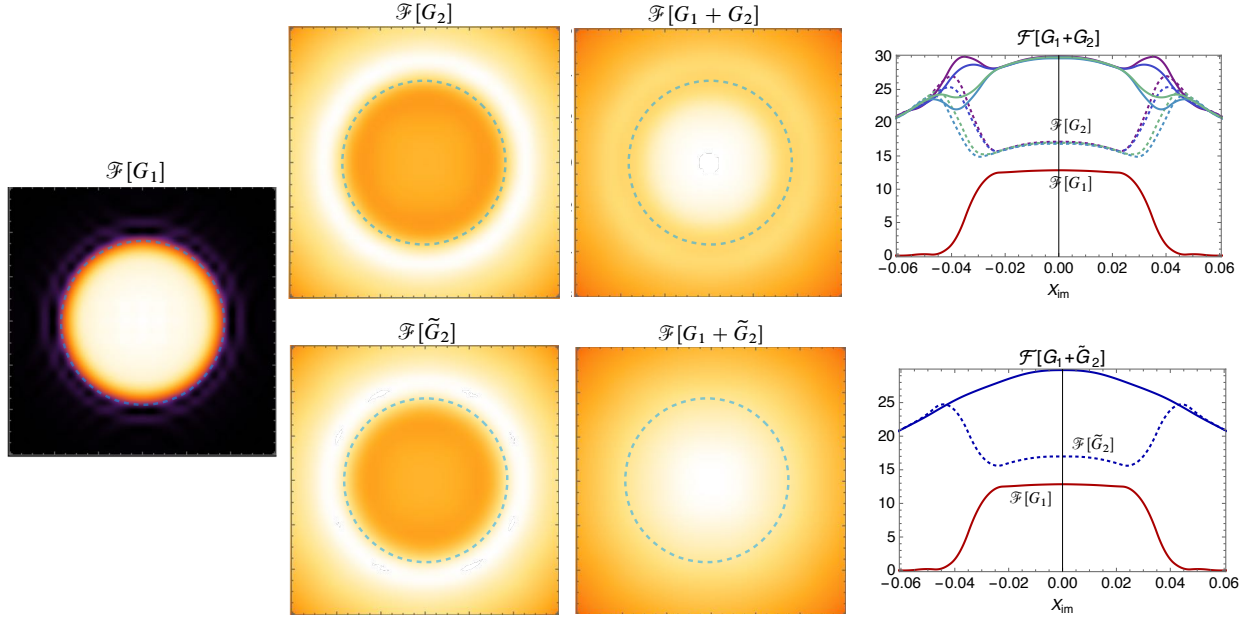


FIG. 6: Images for  $a = 0, \omega = 5$ . Two dimensional images with  $\delta = 3\pi/2$  and one dimensional slice of images along  $Y_{\text{im}} = 0$  (right panels). Dotted circles in two dimensional images represent the photon sphere. In one dimensional slice of  $\mathcal{F}[G_1 + G_2]$ , images with four different phase  $\delta = 0, \pi/2, \pi, 3\pi/2$  are shown.

Figures 7 and 8 shows  $\omega = 0.5$  case. From  $|\tilde{\mathcal{T}}_{\omega\ell m}|$  and  $\mathcal{R}_{\omega\ell m}$ ,  $\ell_* \approx 2$  corresponds to the location of the photon sphere but its shape becomes hazy for low frequency. The image of  $G_1$  spreads over the field of view and structure of the photon sphere is not visible as an image. This is because small  $\ell$  modes mainly contribute to  $G_1$  for low frequency case. The image of  $G$  shows the whole field of view region becomes bright and its brightness is much larger than  $\omega = 5$  case because emission of Hawking radiation is mainly supported by low frequency mode  $\omega \sim \kappa_+/(2\pi)$  of which wavelength is much larger than the size of the photon sphere.

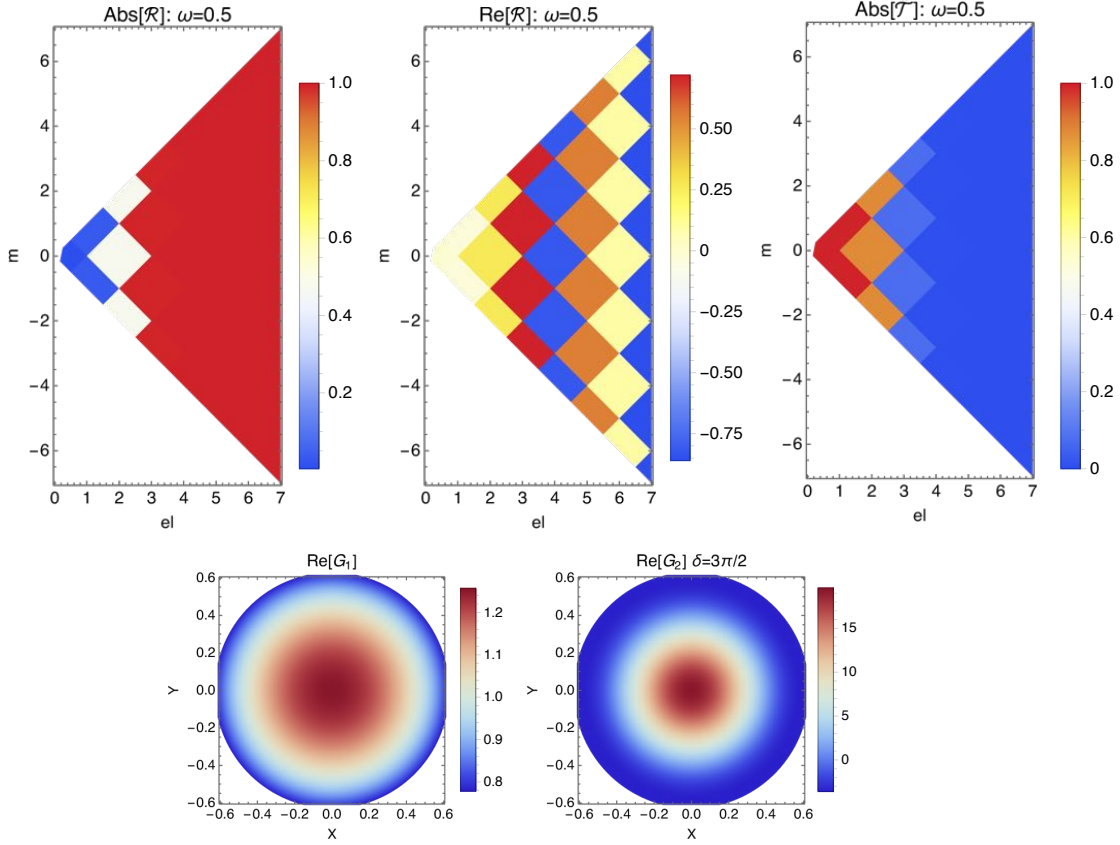


FIG. 7: Reflection and transmission coefficients in  $(\ell, m)$ -plane (upper panels) and  $G_1, G_2$  (lower panels) for  $a = 0, \omega = 0.5$ . Imaginary part of  $G_{1,2}$  is zero.

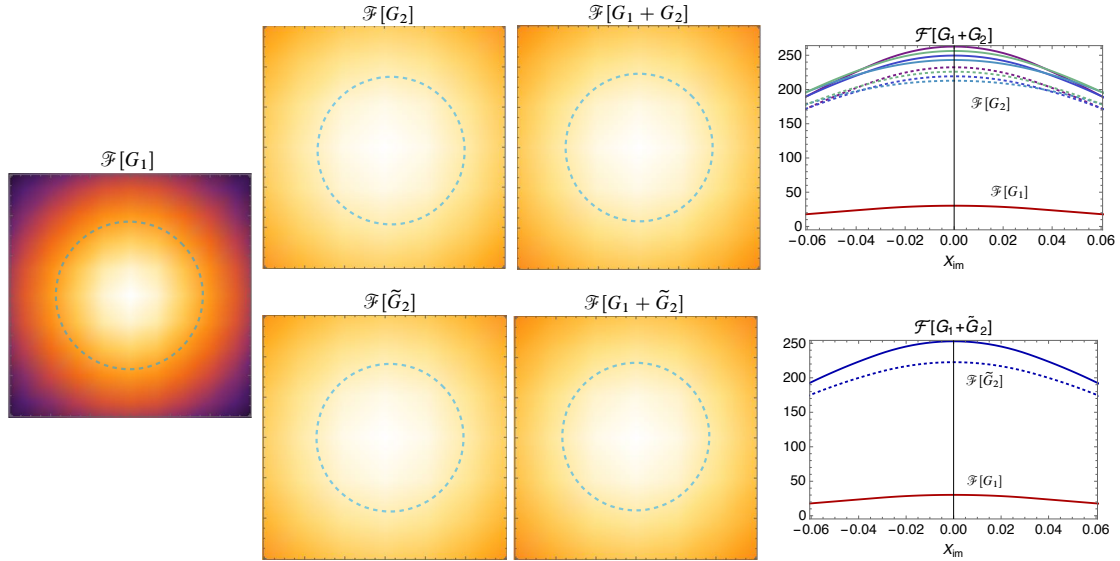


FIG. 8: Images for  $a = 0, \omega = 0.5$ . Two dimensional images are drawn with  $\delta = 3\pi/2$ . Dotted circles in two dimensional images represent the photon sphere. Whole field of view region becomes bright and it is not possible to identify the structure of the photon sphere.

## 2. Images for $a = 1/10$ (slowly rotating case)

Figures 9 and 10 show reflection, transmission coefficients and images for  $a = 1/10, \omega = 5$ . Introduction of small spin results in small deformation of  $\mathcal{R}_{\omega\ell m}$  and  $\tilde{\mathcal{T}}_{\omega\ell m}$  and causes  $m$  dependence of these coefficients. Small spin parameter derives nonzero imaginary part of  $G_{1,2}$  which shows left-right asymmetric fringe pattern in the observer's screen. Image of  $G_1$  shows the spherical photon sphere which is not possible to distinguish it from the image of  $a = 0$  case. However, images of  $G_2$  shows irregular shaped ring which is caused by interference effect between incoming and outgoing waves. Indeed, image of  $\tilde{G}_2$  shows circular shaped ring of the photon sphere. Moreover, the interference effect enhances left-right asymmetry of intensity of images around the photon sphere, which is clearly visible from the one dimensional slice of images (right panels of Fig. 10).

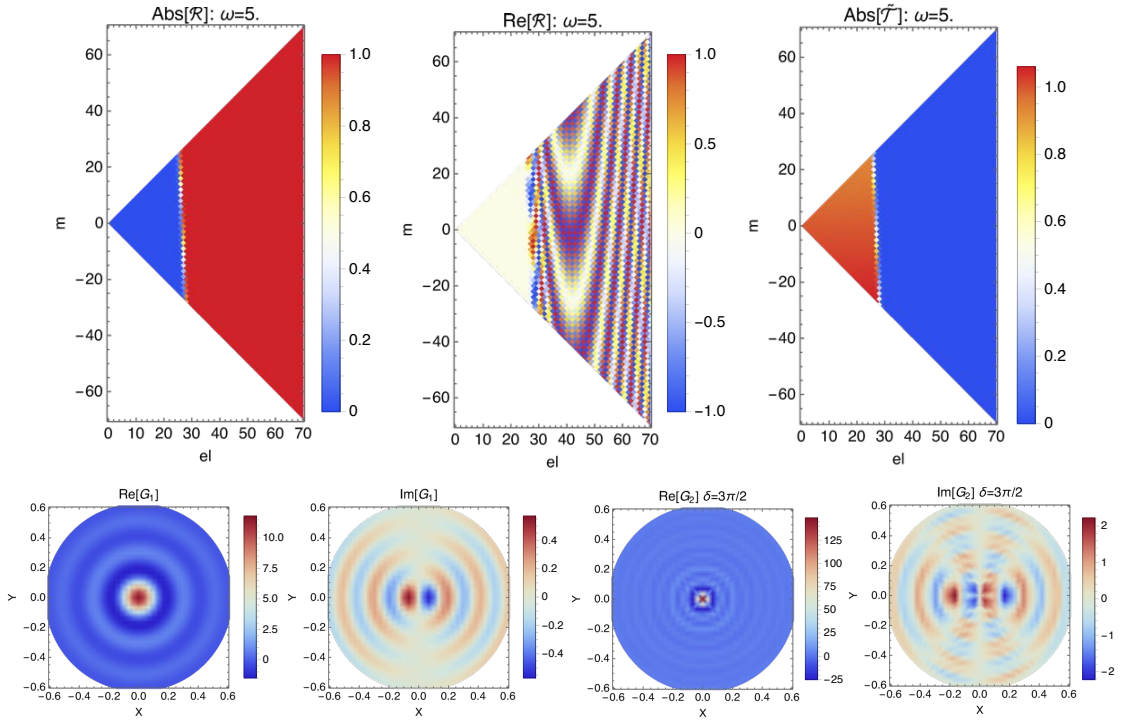


FIG. 9: Reflection and transmission coefficients in  $(\ell, m)$ -plane (upper panels) and  $G_1, G_2$  (lower panels) for  $a = 0.1, \omega = 5$ . Reflection and transmission coefficients show  $m$  dependence. Imaginary part of  $G_{1,2}$  presents left-right asymmetric fringe patterns which are caused by small value of the spin parameter.

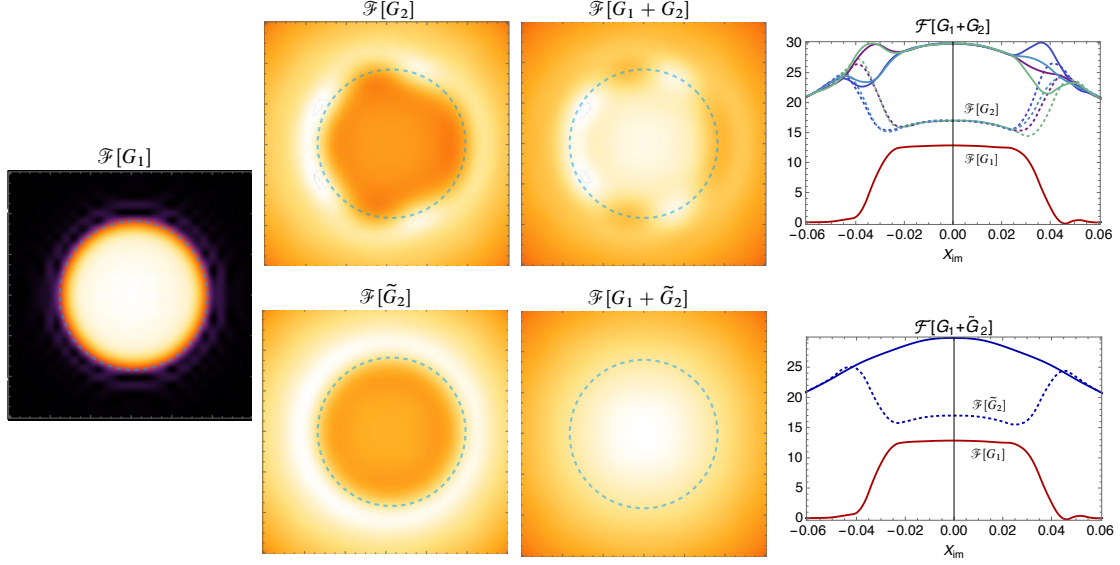


FIG. 10: Images for  $a = 1/10, \omega = 5$ . Two dimensional images are with  $\delta = 3\pi/2$ . Dotted circles in two dimensional images represent the photon sphere. Asymmetry of  $\mathcal{F}[G_2]$  and  $\mathcal{F}[G_1 + G_2]$  reflect effect of small nonzero value of the spin parameter.

Figures 11 and 12 show reflection, transmission coefficients and images for  $a = 1/10, \omega = 0.5$ .  $|\tilde{\mathcal{T}}_{\omega\ell m}|$  and  $\mathcal{R}_{\omega\ell m}$  show small  $m$  dependence. For  $\ell$  dependence, it is not possible to distinguish it from  $a = 0, \omega = 0.5$  case. Small  $a$  induces imaginary part of  $G$  which shows left-right asymmetry. We cannot recognize shape of the emission region of Hawking radiation (Fig. 12). The effect of small spin parameter is visible as small left-right asymmetry in the one-dimensional intensity distribution (right panel of Fig. 12).

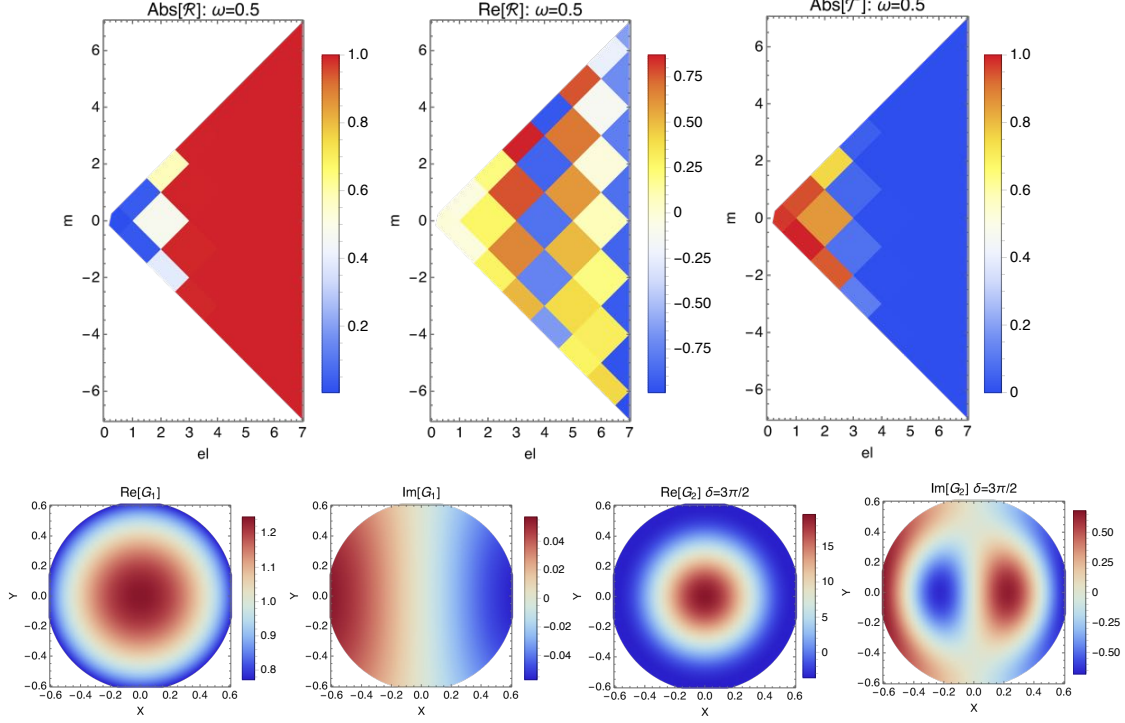


FIG. 11: Reflection and transmission coefficients in  $(\ell, m)$ -plane (upper panels) and  $G_1, G_2$  (lower panels) for  $a = 1/10, \omega = 0.5$ . Left-right asymmetry of fringe patterns of  $\text{Im}[G_1]$  and  $\text{Im}[G_2]$  is also seen for low frequency case.

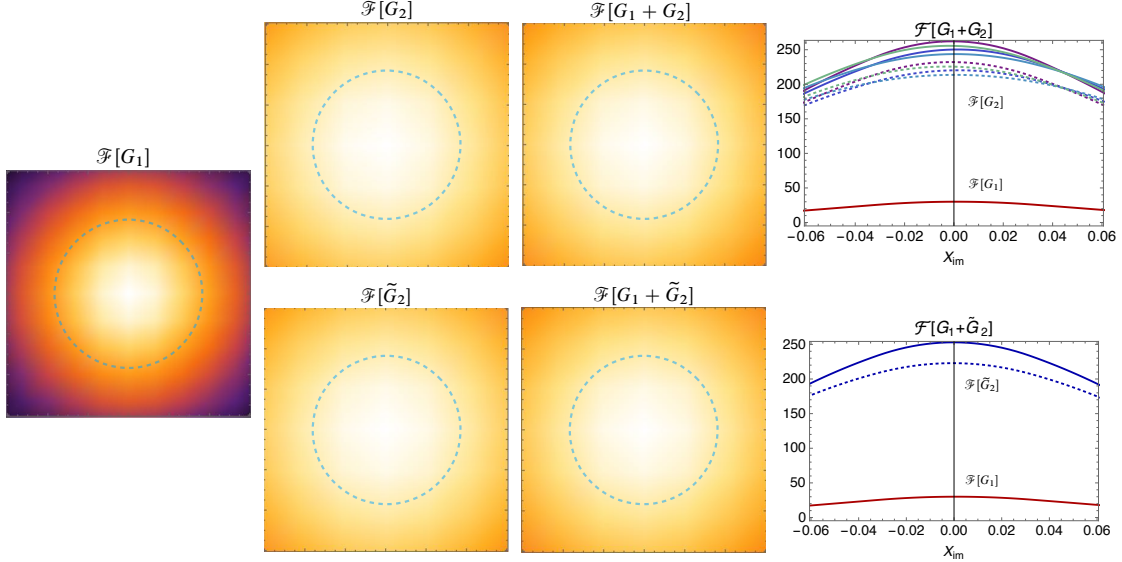


FIG. 12: Images for  $a = 1/10, \omega = 0.5$ . Two dimensional images are with  $\delta = 3\pi/2$ . Dotted circles in two dimensional images represent the photon sphere. Left-right asymmetry is visible in  $\mathcal{F}[G_1 + G_2]$ .

### 3. Images for $a = 1$ (fast rotating case)

Figure 13 shows transmission, reflection coefficients for  $a = 1, \omega = 5$ . Transmission and reflection coefficients show larger  $m$  dependence compared to  $a = 0.1$  case and the boundary between perfect reflection and absorption is much deformed from a  $\ell = \text{constant}$  line. This reflects non-spherical shape of the photon sphere. The interference fringe pattern  $\text{Re}[G_1]$  is elongated to the  $Y$  direction and becomes elliptic shape due to the spin of the black hole. Although superradiant modes are included in the sum of the correlation function, impact of these modes on images is not visible due to smallness of amplification factor for the scalar mode superradiance.

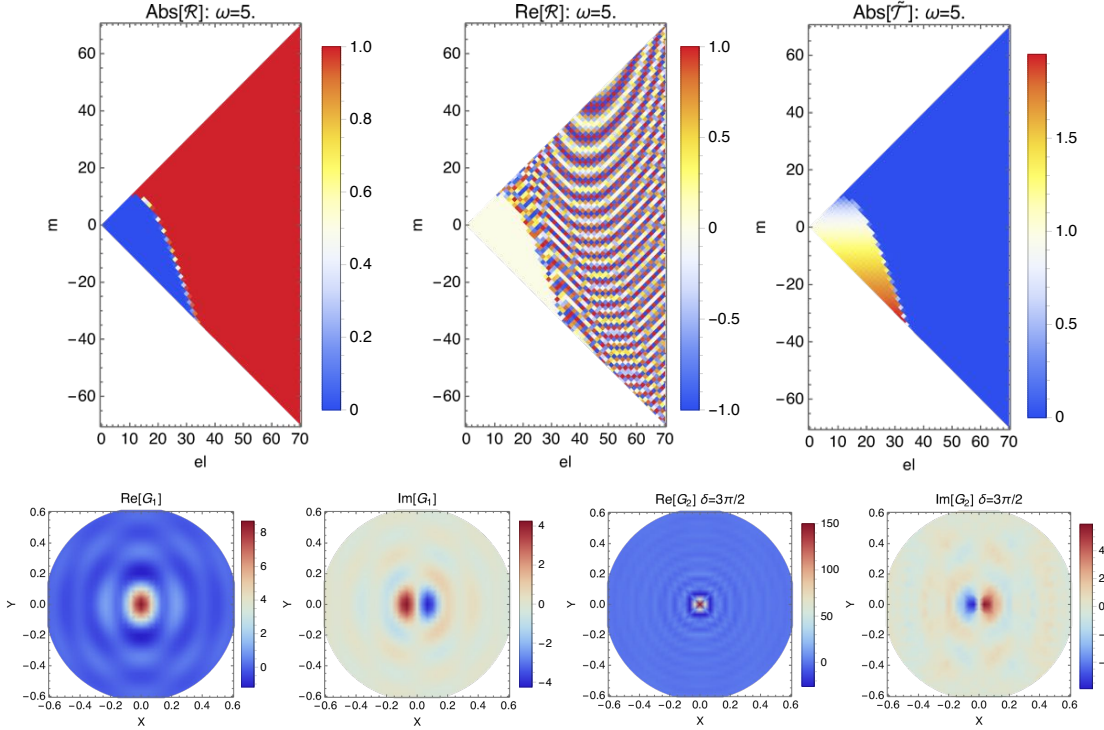


FIG. 13: Reflection and transmission coefficients in  $(\ell, m)$ -plane (upper panels) and  $G_1, G_2$  (lower panels) for  $a = 1, \omega = 5$ . The interference fringe pattern  $\text{Re}[G_1]$  is elongated to the  $Y$  direction and becomes elliptic shape due to the spin of the black hole.

Figure 14 shows images obtained from  $G$ . The image of  $G_1$  shows a deformed D-shaped region corresponding to shape of the photon sphere. The intensity inside of the photon sphere slightly decreases as  $X_{\text{im}}$  increases due to the dragging effect of the Kerr black hole. The image of  $G_2$  shows a dark shadow region caused by absorption of the incoming radiation from the cosmological horizon by the black hole. A peculiar feature of this image is existence of a bright spot at the left side of the photon sphere; this enhancement of the intensity is due to interference effect because we cannot find out the enhancement of intensity in the image of  $\tilde{G}_2$ . As we can see from the one dimensional slice of images (right panels of Fig. 14), the right side of the photon sphere can also become bright depending on the value of  $\delta$ . However, contrast of intensity at the left side is larger than that of the right side and this difference is due to the dragging effect of the Kerr black hole.

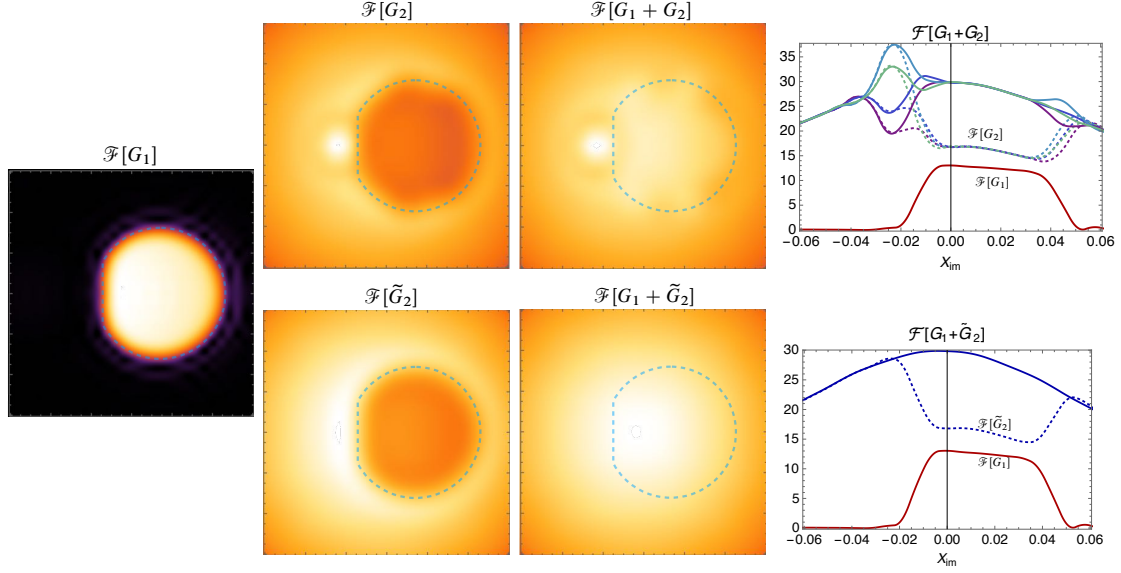


FIG. 14: Images for  $a = 1, \omega = 5$ . Dotted circles in two dimensional images represent the photon sphere.  $\mathcal{F}[G_2]$  and  $\mathcal{F}[G_1 + G_2]$  are images with  $\delta = 3\pi/2$  and they show bright spots at the left side of the photon sphere which are caused by interference between incoming modes and reflected modes.

Figure 15 and 16 show transmission, reflection coefficients and images  $a = 1, \omega = 0.5$ . Although we cannot identify the photon sphere in images, left-right asymmetry of intensity caused by the dragging effect of fast rotation of the black hole is visible.

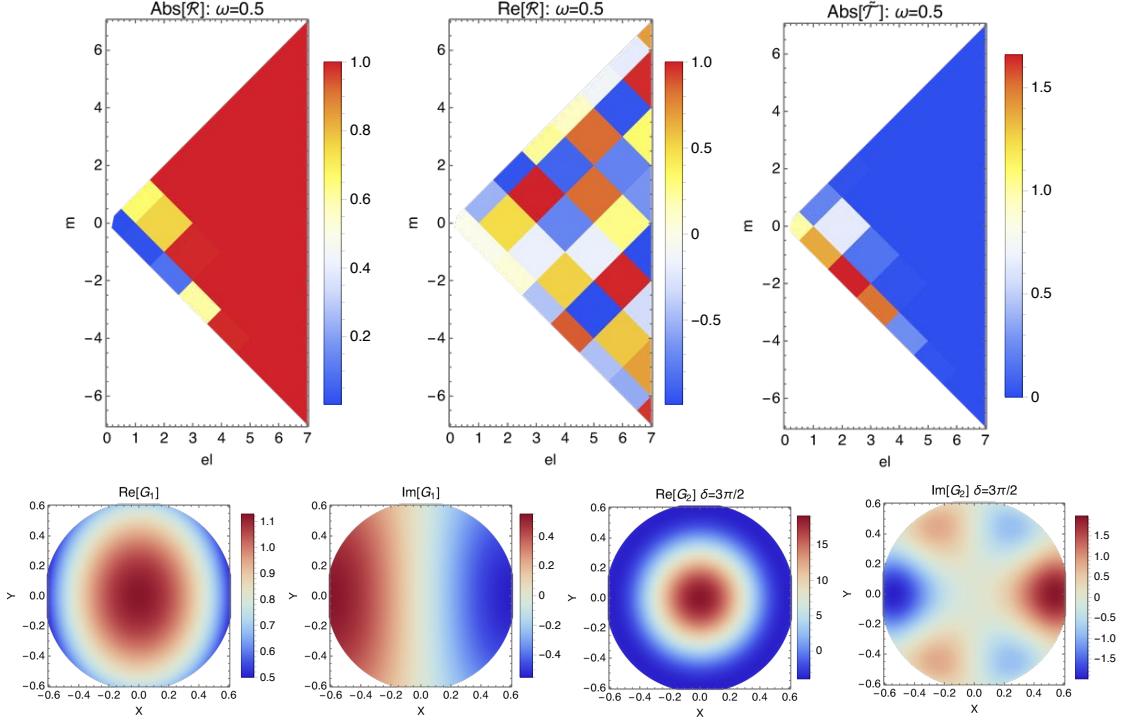


FIG. 15: Reflection and transmission coefficients in  $(\ell, m)$ -plane (upper panels) and  $G_1, G_2$  (lower panels) for  $a = 1, \omega = 0.5$ .  $\text{Im}[G_{1,2}]$  shows left-right asymmetry due to spin of the black hole.

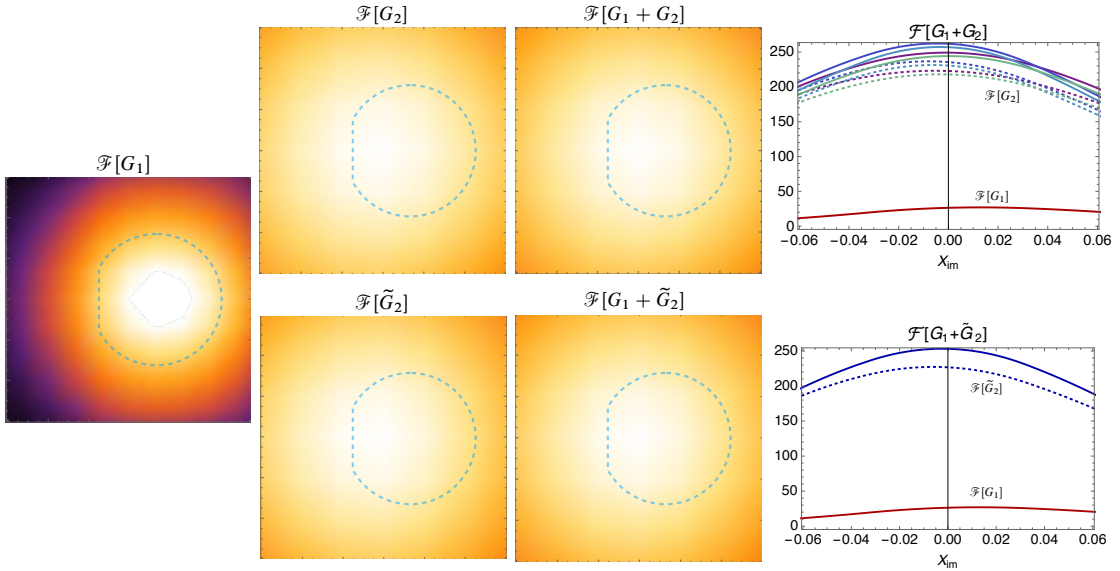


FIG. 16: Images for  $a = 1, \omega = 0.5$ . Two dimensional images are with  $\delta = 3\pi/2$ . Dotted circles in two dimensional images represent the photon sphere.  $\mathcal{F}[G_2]$  and  $\mathcal{F}[G_1 + G_2]$  are images with  $\delta = 3\pi/2$ . Left-right asymmetry is visible in one dimensional slice of  $\mathcal{F}[G_1 + G_2]$ .

#### 4. Images of $G_1$ and emission region of Hawking radiation

Figure 17 shows one dimensional slice of images  $\mathcal{F}[G_1]$  with different frequencies. For  $\omega = 5$ , we can identify the location of photon sphere which is visible as sharp edges of image. The size of effective emission area of Hawking radiation is same as the size of the photon sphere as discussed in [13, 14]. For low frequency, the effective size of radiation source obtained from images becomes larger than the photon sphere. This is because  $\ell = 0$  mode mainly contributes in the greybody factor  $|\tilde{T}_{\omega\ell m}|^2$  for  $\omega \rightarrow 0$  and characteristic size of emission region depends on  $\omega$ . Introduction of the spin does not alter this behavior of  $\omega$  dependence of the size of emission region of Hawking radiation.

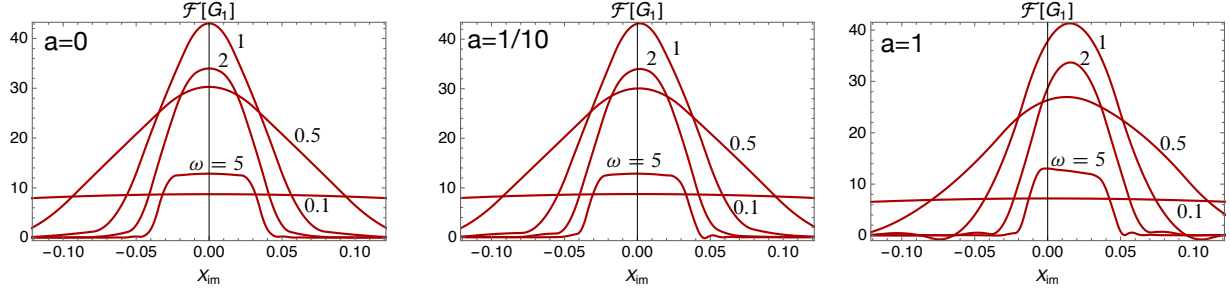


FIG. 17: Slices of images  $\mathcal{F}[G_1]$  along the  $Y_{\text{im}} = 0$  line. For lower frequencies, the effective size of emission region becomes larger than the photon sphere.

For the purpose of obtaining black hole images directly related to emission of Hawking radiation, we consider images with the UP mode for the correlation function  $G_1 - G_1^{\text{Boulware}}$  given by Eq. (52) which subtracts contribution of the vacuum fluctuation (Fig. 18). Obtained images are sensitive to values of the spin parameter. For  $a \neq 0$ , owing to  $m$ -dependence of the Planckian factor in (52), intensity of small emission region around the left side of the photon sphere becomes large and decays exponentially as departs from this region. Peak intensity of the emission region strongly depend on the spin parameter:  $9.5 \times 10^{-49}$  for  $a = 0.1$  and  $4.8 \times 10^{-10}$  for  $a = 1$ . As this  $m$ -dependence in the Planckian factor is proportional to the angular velocity of the black hole, images of  $G_1 - G_1^{\text{Boulware}}$  reflect the dragging effect in the vicinity of the event horizon of the Kerr black hole.

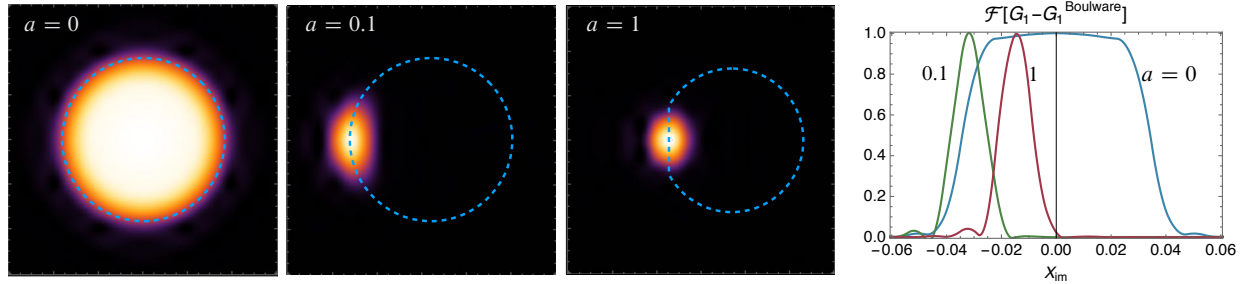


FIG. 18: Images of the UP mode for  $G_1 - G_1^{\text{Boulware}}$  with  $\omega = 5$ . Dotted circles denote the photon sphere. The right panel is one dimensional slice of images along  $Y_{\text{im}} = 0$ . The intensity is normalized by its peak value. Unnormalized values of intensity are  $5.1 \times 10^{-57}$  for  $a = 0$ ,  $9.5 \times 10^{-49}$  for  $a = 0.1$  and  $4.8 \times 10^{-10}$  for  $a = 1$ .

## VI. SUMMARY

We investigate wave optical imaging of black holes using Hawking radiation. Concerning theoretical investigation on imaging of astrophysical black holes, Falcke *et al.* [34] obtained images of black hole shadows using the ray tracing of photons emitted from infalling gas around the Kerr black hole. Their images show left-right asymmetry of intensity due to the spin of the black hole and frequency dependence of images that the “shadow” becomes invisible for low frequency due to scattering of photons by plasma around the black hole. Comparing their images with ours obtained in this paper, apparent structure of our images  $\mathcal{F}[G_2]$  (in Figs. 14 and 16) resembles theirs. However, images  $\mathcal{F}[G_1 + G_2]$  show no specific structure associated with the photon sphere. As discussed in Section V A, for high frequency waves larger than the Hawking temperature, the structure of image  $\mathcal{F}[G_1 + G_2]$  becomes flat if we neglect the interference effect. In our calculation, adopted frequency is far higher than the Hawking temperature  $\omega_+ \approx 0.006, \omega_c \approx 0.008$  for  $a = 1$  and this is why we do not have shadow images for  $\mathcal{F}[G_1 + G_2]$ . Although it is not possible to identify the exact location of wave source for Hawking radiation, we applied the van Citter-Zernike theorem and obtained projected two dimensional images of the black hole via Fourier transformation of spatial correlation functions. Obtained images trace shape of the photon sphere of the black hole for high frequency and we see the black hole looks like a shining star with the photon sphere as its surface. For low frequency, a definite surface of emission is lost and emission region extends over whole field of view larger than the size of the photon sphere. We found that interference between incoming modes from the cosmological horizon and reflected modes by the black hole enhances intensity of images in the vicinity of the photon sphere for fast spinning case.

We are not certain whether the “source” region of Hawking radiation is spatial incoherent which is crucial to assumption of the van Citter-Zernike theorem for imaging of black holes with Hawking radiation. However, even though detail of the spatial incoherence is not justified, it is possible to adopt Fourier transformation of the spatial correlation function as a tool to visualize black holes with Hawking radiation. The spatial correlation function of the up mode near the black hole (near the past event horizon) is roughly estimated as follows; the radial wave function in the vicinity of the horizon is  $R_{\ell m}^{\text{up}} \sim e^{-i(\omega - m\Omega)r_*}$ , and

$$G_1(\theta_1, \phi_1, \theta_2, \phi_2) \sim \sum_{\ell m} |R_{\ell m}^{\text{up}}(r)|^2 S_{\ell m}(\theta_1) S_{\ell m}(\theta_2) e^{im(\phi_1 - \phi_2)} \sim \delta(\theta_1 - \theta_2) \delta(\phi_1 - \phi_2), \quad (84)$$

because  $|R_{\omega \ell m}^{\text{up}}|^2$  does not have  $\ell, m$  dependence. Therefore, if we assume that Hawking radiation is emitted from  $r = \text{constant}$  surface in the vicinity of the horizon, the spatial coherence on that source surface is zero and we have justified applicability of the van Citter-Zernike theorem to imaging with Hawking radiation. Emission region of Hawking radiation may differs from the vicinity of the horizon and for such a case we cannot say definite thing on spatial incoherence of the source region of Hawking radiation. Spatial incoherence of the source will result in hazy images and more rigorous investigation with the effect of spatial coherent source will unveil “quantumness” of Hawking radiation. The word “quantumness” is obscure and we should provide definite meaning of it based on entanglement. If we reconsider the van Citter-Zernike theorem for a source with spatial coherence, it can be possible to access information on the degree of coherence of Hawking radiation. This direction of investigation is related to entanglement harvesting in black hole spacetimes with the method of intensity correlation [35] and we will report this subject in a separate publication.

## Acknowledgments

Y.N. was supported in part by JSPS KAKENHI Grant No. 19K03866.

- 
- [1] V. P. Frolov and I. D. Novikov, *Black Hole Physics* (Kluwer Academic Publisher, Dordrecht, Netherlands, 1998).
  - [2] The Event Horizon Telescope Collaboration, “First M87 Event Horizon Telescope Results. I. The Shadow of the Supermassive Black Hole”, *Astrophys. J.* **875**, (2019) L1.
  - [3] The Event Horizon Telescope Collaboration, “First M87 Event Horizon Telescope Results. II. Array and Instrumentation”, *Astrophys. J.* **875**, (2019) L2.
  - [4] The Event Horizon Telescope Collaboration, “First M87 Event Horizon Telescope Results. III. Data Processing and Calibration”, *Astrophys. J.* **875**, (2019) L3.
  - [5] The Event Horizon Telescope Collaboration, “First M87 Event Horizon Telescope Results. IV. Imaging the Central Supermassive Black Hole”, *Astrophys. J.* **875**, (2019) L4.
  - [6] The Event Horizon Telescope Collaboration, “First M87 Event Horizon Telescope Results. V. Physical Origin of the Asymmetric Ring”, *Astrophys. J.* **875**, (2019) L5.
  - [7] The Event Horizon Telescope Collaboration, “First M87 Event Horizon Telescope Results. VI. The Shadow and Mass of the Central Black Hole”, *Astrophys. J.* **875**, (2019) L6.
  - [8] M. Born and E. Wolf, *Principles of Optics* (Cambridge University Press, 1999), 7th ed.
  - [9] E. Wolf, *Introduction to the theory of coherence and polarization of light* (Cambridge University Press, 2007).
  - [10] K. Sharma, *Optics: principles and applications* (Academic Press, Tokyo, 2006).
  - [11] S. W. Hawking, “Black hole explosions?”, *Nature* **248**, (1974) 30–31.
  - [12] S. W. Hawking, “Particle creation by black holes”, *Commun. Math. Phys.* **43**, (1975) 199–220.
  - [13] S. B. Giddings, “Hawking radiation, the Stefan-Boltzmann law, and unitarization”, *Phys. Lett. B* **754**, (2016) 39–42.
  - [14] R. Dey, S. Liberati, and D. Pranzetti, “The black hole quantum atmosphere”, *Phys. Lett. B* **774**, (2017) 308–316.
  - [15] K.-i. Kanai and Y. Nambu, “Viewing black holes by waves”, *Class. Quantum Gravity* **30**, (2013) 175002.
  - [16] Y. Nambu and S. Noda, “Wave optics in black hole spacetimes: the Schwarzschild case”, *Class. Quantum Gravity* **33**, (2016) 075011.
  - [17] W. G. W. Unruh, “Notes on black-hole evaporation”, *Phys. Rev. D* **14**, (1976) 870–892.
  - [18] P. Candelas, “Vacuum polarization in Schwarzschild spacetime”, *Phys. Rev. D* **21**, (1980) 2185–2202.
  - [19] A. C. Ottewill and E. Winstanley, “Renormalized stress tensor in Kerr space-time: General results”, *Phys. Rev. D* **62**, (2000) 1–15.
  - [20] R. Gregory, I. G. Moss, N. Oshita, and S. Patrick, “Black hole evaporation in de Sitter space”, *arXiv:2103.09862* .
  - [21] N. D. Birrell and P. C. W. Davies, *Quantum fields in curved space* (Cambridge University Press, 1984).
  - [22] B. Reznik, “Entanglement from the vacuum”, *Found. Phys.* **33**, (2003) 167–176.
  - [23] A. Pozas-Kerstjens and E. Martín-Martínez, “Harvesting correlations from the quantum vacuum”, *Phys. Rev. D* **92**, (2015) 064042.

- [24] L. J. Henderson, R. A. Hennigar, R. B. Mann, A. R. H. Smith, and J. Zhang, “Harvesting entanglement from the black hole vacuum”, *Class. Quantum Gravity* **35**, (2018) 21LT02.
- [25] Y. Nambu and Y. Ohsumi, “Classical and quantum correlations of scalar field in the inflationary universe”, *Phys. Rev. D* **84**, (2011) 044028.
- [26] A. Matsumura and Y. Nambu, “Violation of Bell-CHSH Inequalities through Optimal Local Filters in the Vacuum”, *Quantum Reports* **2**, (2020) 542–559.
- [27] G. Vidal and R. Werner, “Computable measure of entanglement”, *Phys. Rev. A* **65**, (2002) 032314.
- [28] E. Tjoa and R. B. Mann, “Harvesting correlations in Schwarzschild and collapsing shell spacetimes”, *J. High Energy Phys.* **2020 (8)**, (2020) 155.
- [29] G. Menezes, “Entanglement dynamics in a Kerr spacetime”, *Phys. Rev. D* **97**, (2018) 85021.
- [30] S. Akcay and R. A. Matzner, “The Kerr–de Sitter universe”, *Class. Quantum Gravity* **28**, (2011) 085012.
- [31] Y. Hatsuda, “Quasinormal modes of Kerr–de Sitter black holes via the Heun function”, *Class. Quantum Gravity* **38**, (2021) 025015.
- [32] H. Motohashi and S. Noda, “Exact solution for wave scattering from black holes: Formulation”, *Prog. Theor. Exp. Phys.* **2021 (8)**, (2021) 1–27.
- [33] H. Suzuki, E. Takasugi, and H. Umetsu, “Perturbations of Kerr-de Sitter Black Holes and Heun’s Equations”, *Prog. Theor. Phys.* **100**, (1998) 491–505.
- [34] H. Falcke, F. Melia, and E. Agol, “Viewing the Shadow of the Black Hole at the Galactic Center”, *Astrophys. J.* **528**, (2000) L13–L16.
- [35] G. Baym, “The physics of Hanbury Brown-Twiss intensity interferometry: From stars to nuclear collisions”, *Acta Phys. Pol. B* **29**, (1998) 1839–1884.